

Accepted Manuscript

Structural optimization of diphenylpyrimidine derivatives (DPPYs) as potent Bruton's tyrosine kinase (BTK) inhibitors with improved activity toward B leukemia cell lines

Dan Zhao, Shanshan Huang, Menghua Qu, Changyuan Wang, Zhihao Liu, Zhen Li, Jinyong Peng, Kexin Liu, Yanxia Li, Xiaodong Ma, Xiaohong Shu



PII: S0223-5234(16)30985-0

DOI: [10.1016/j.ejmech.2016.11.047](https://doi.org/10.1016/j.ejmech.2016.11.047)

Reference: EJMECH 9080

To appear in: *European Journal of Medicinal Chemistry*

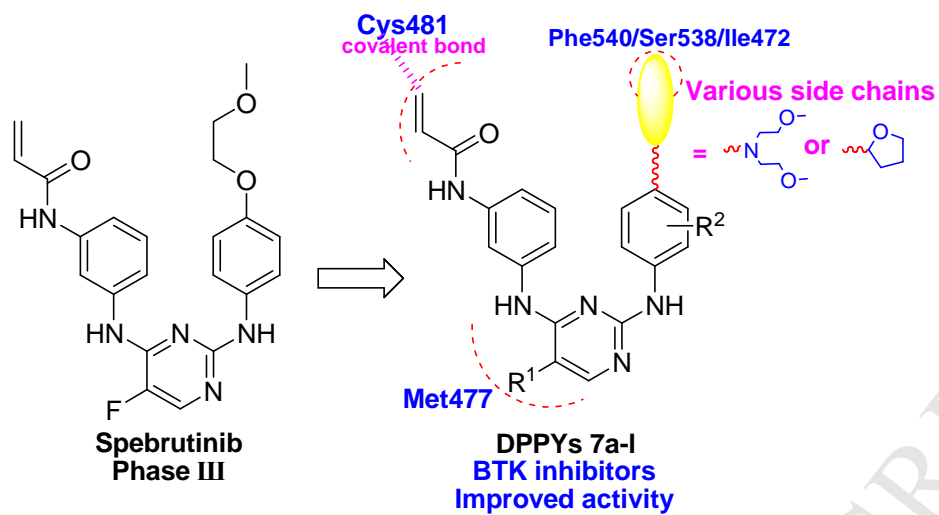
Received Date: 4 September 2016

Revised Date: 20 November 2016

Accepted Date: 21 November 2016

Please cite this article as: D. Zhao, S. Huang, M. Qu, C. Wang, Z. Liu, Z. Li, J. Peng, K. Liu, Y. Li, X. Ma, X. Shu, Structural optimization of diphenylpyrimidine derivatives (DPPYs) as potent Bruton's tyrosine kinase (BTK) inhibitors with improved activity toward B leukemia cell lines, *European Journal of Medicinal Chemistry* (2016), doi: 10.1016/j.ejmech.2016.11.047.

This is a PDF file of an unedited manuscript that has been accepted for publication. As a service to our customers we are providing this early version of the manuscript. The manuscript will undergo copyediting, typesetting, and review of the resulting proof before it is published in its final form. Please note that during the production process errors may be discovered which could affect the content, and all legal disclaimers that apply to the journal pertain.



**Structural optimization of diphenylpyrimidine derivatives
(DPPYs) as potent Bruton's tyrosine kinase (BTK) inhibitors
with improved activity toward B leukemia cell lines**

Dan Zhao^a, Shanshan Huang^a, Menghua Qu^a, Changyuan Wang^a, Zhihao Liu^a, Zhen Li^a,
Jinyong Peng^a, Kexin Liu^a, Yanxia Li^b, Xiaodong Ma^{a,*}, and Xiaohong Shu^{a,*}

^a College of Pharmacy, Dalian Medical University, Dalian 116044, PR China.

^b Department of Respiratory Medicine, the First Affiliated Hospital of Dalian Medical University, Dalian 116011, PR China.

E-mail address: xiaodong.ma@139.com (X.D. Ma), xiaohong_shu@dmu.edu.cn (X.H. Shu).

Abstract

A new series of diphenylpyrimidine derivatives (DPPYs) bearing various aniline side chains at the C-2 position of pyrimidine core were synthesized as potent BTK inhibitors. Most of these inhibitors displayed improved activity against B leukemia cell lines compared with lead compound spebrutinib. Subsequent studies showed that the peculiar inhibitor **7j**, with IC₅₀ values of 10.5 μM against Ramos cells and 19.1 μM against Raji cells, also displayed slightly higher inhibitory ability than the novel agent ibrutinib. Moreover, compound **7j** is not sensitive to normal cells PBMC, indicating low cell cytotoxicity. In addition, flow cytometry analysis indicated that **7j** significantly induced the apoptosis of Ramos cells, and arrested the cell cycle at the G0/G1 phase. These explorations provided new clues to discover pyrimidine scaffold as more effective BTK inhibitors.

Keywords: Leukemia; BTK; Pyrimidine; Synthesis; Inhibitor.

1. Introduction

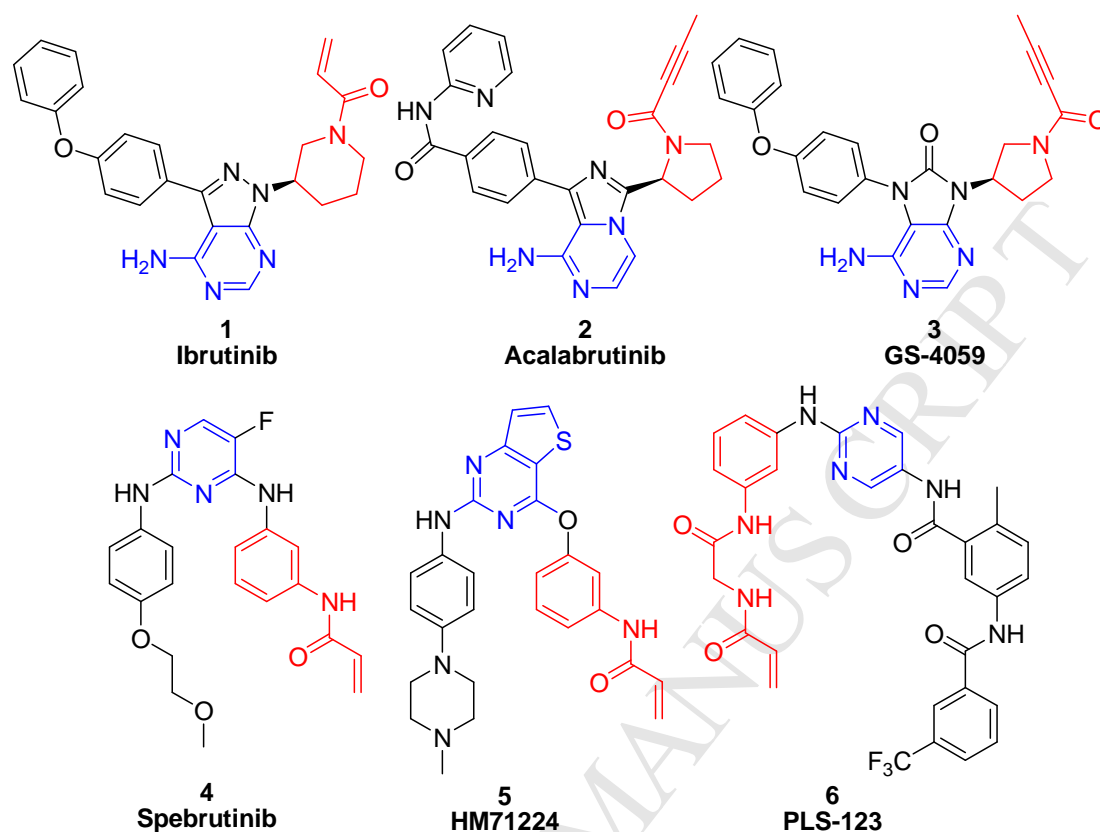


Fig. 1. Structures of the novel BTK inhibitors.

Bruton's tyrosine kinase (BTK), a key member of the Tec family of non-receptor tyrosine kinases, plays an important role in the B-cell signaling pathway linking cell surface B-cell receptor (BCR) stimulation to downstream intracellular responses [1-3]. It has been reported that numerous B-cell-derived malignancies, such as acute lymphoblastic leukemia (ALL), chronic lymphocytic leukemia (CLL), non-Hodgkin's lymphoma (NHL), mantle cell lymphoma (MCL), Waldenström's Macroglobunemia (WM) and multiple myeloma (MM), are related to the deregulation of BTK kinase [4,5]. Till now, considerable efforts focused on searching for effective agents against various B-cell-derived tumors have brought promising prospect for cancer patients [6]. Inspiringly, a clinically advanced irreversible BTK kinase inhibitor, ibrutinib, which has demonstrated efficacy in patients with CLL, MCL, WM and MCL, has been broadly used in clinical [6-9]. Recently, a number of novel covalent and noncovalent BTK inhibitors, including acalabrutinib (2) (ClinicalTrials.gov identifier: NCT02717611) [10-12], GS-4059 (3) (ClinicalTrials.gov identifier: NCT02457559) [13,14], spebrutinib (4) (ClinicalTrials.gov identifier: NCT01744626) [15], HM71224

(5) (ClinicalTrials.gov identifier: NCT01765478) [16], and PLS-123 (6) [17], have been advanced to preclinical or clinical trials (Fig. 1).

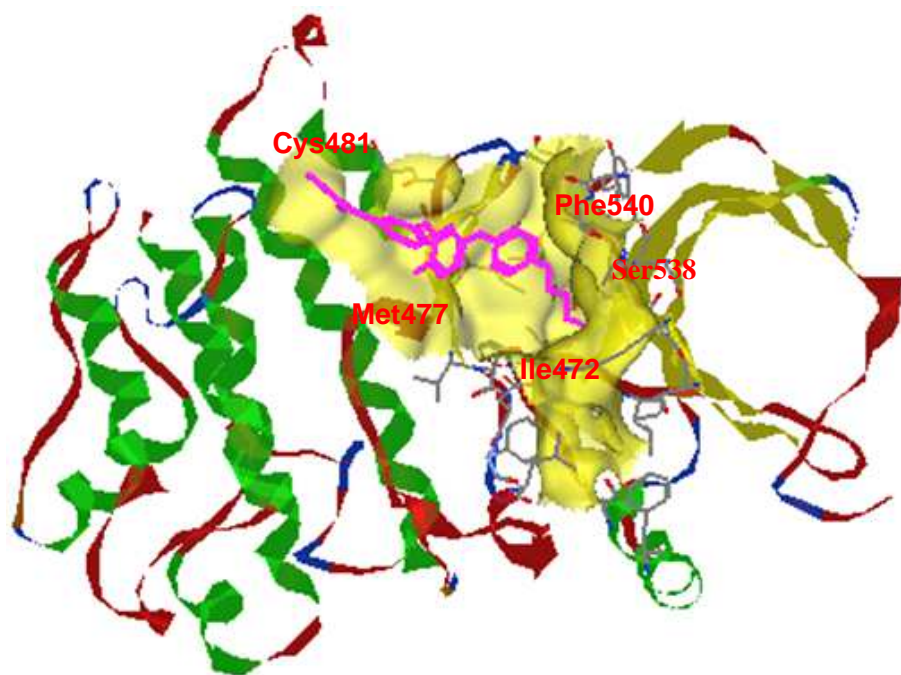


Fig. 2. Binding mode of spebrutinib with BTK enzyme (PDB: 3GEN).

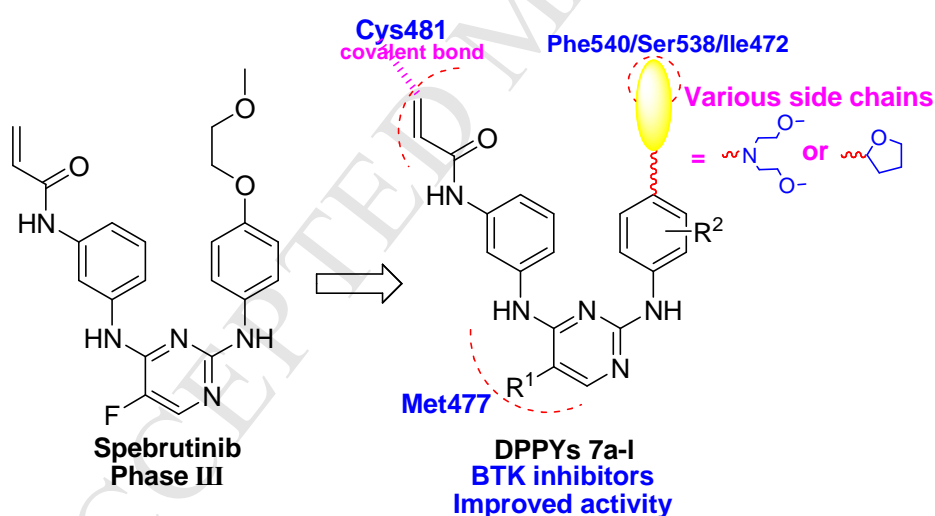


Fig. 3. Designed strategy of new DPPYs as potent BTK inhibitors.

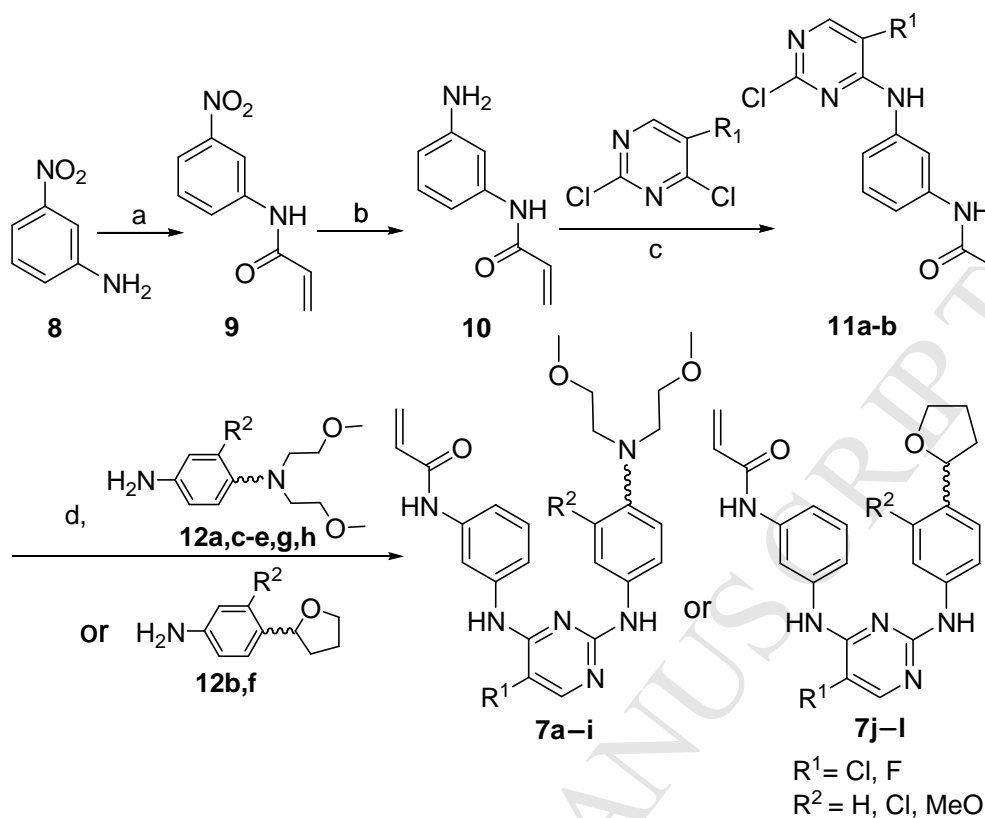
It is clear that these novel BTK inhibitors possess a pyrimidine core, along with a typical *N*-phenylacrylamide functionality. Previous structure and activity relationships (SARs) explorations showed that the acryloyl group was essential to form a covalent bond with the amino acid Cys481 of BTK, while a *C*-4'-substituted aniline side chain installed on the *C*-2 position of pyrimidine core was also beneficial to form contacts with the residues Phe540, Ile472, Ser538, Lys430 at the bottom of the ATP-binding

pocket (Fig. 2) [7,18-20]. To improve the binding affinity with BTK, herein, a series of new dipenylpyrimidine derivatives (DPPYs) **7a-l** bearing various *C*-2 aniline side chains were synthesized and biologically evaluated for their activity against BTK kinase and B lymphoma cell lines (Fig. 3). Accordingly, our molecule simulations showed in Fig. 7 indicated that the newly designed molecules tightly contact with BTK, and which would enhance the activity against BTK.

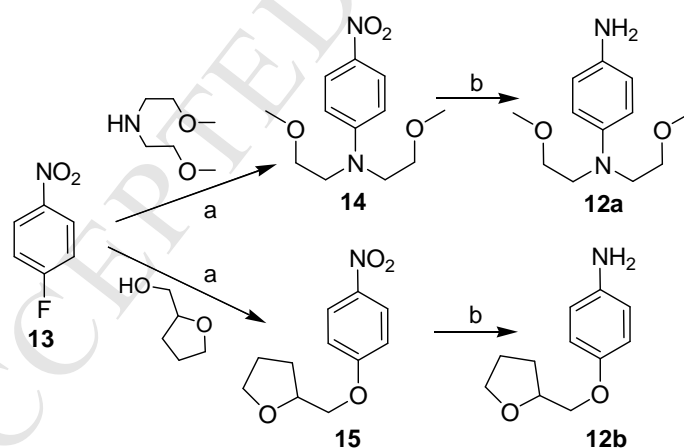
2. Results and Discussion

2.1 Chemistry

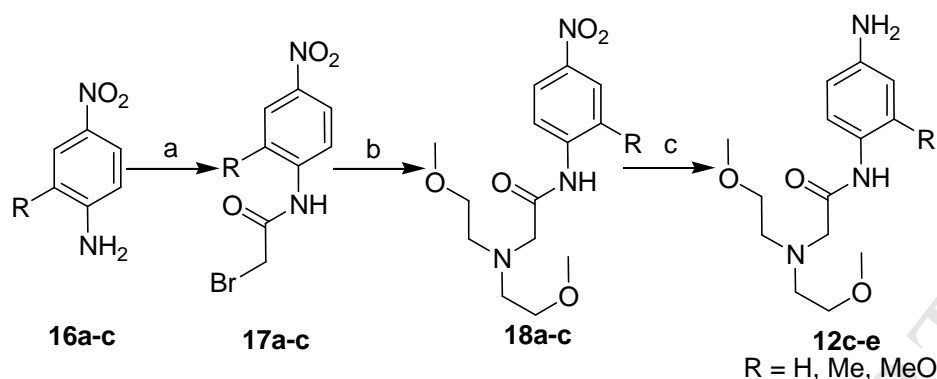
The title molecules **7a-l** were synthesized as depicted in Scheme 1 [21,22]. Starting from 3-nitroaniline (**8**), acylation reaction using acryloyl chloride under basic conditions (NaHCO_3) was furnished to produce *N*-acryloyl-4-nitrobenzamide (**9**). After reduction of the nitro group of compound **9** under Fe- NH_4Cl conditions, the 4-aminobenzamide derivative (**10**) was conveniently synthesized. Compound **10** was regioselectively coupled to the *C*-4 position of 2,4-dichloropyrimidine template to afford the key intermediate **11a-b**. As indicated in Scheme 2-4, various aniline side chains **12a-h** were prepared according to general synthetic methods [23,24], including aromatic nucleophilic substitution, acylation, and reduction reactions, etc. Coupling reactions of **11a-b** with aniline intermediates **12a-h** were accomplished in the presence of trifluoroacetic acid (TFA) under reflux conditions, offering the title molecules **7a-i** and **7j-l** with yield ranging from 31% to 45%.



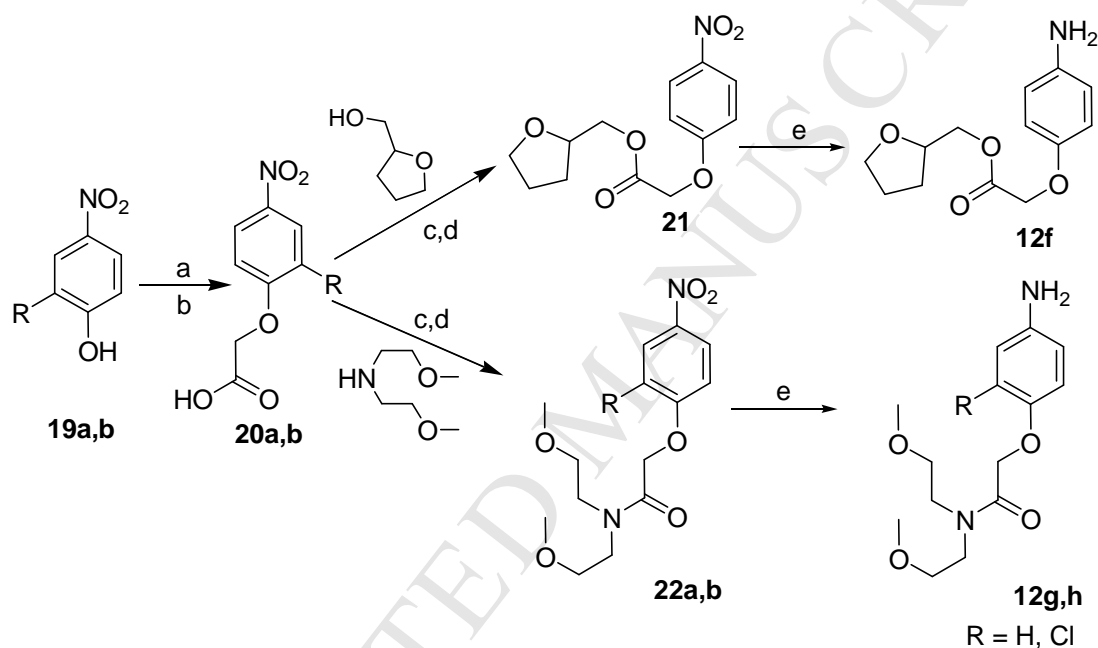
Scheme 1. Synthetic route of title compounds **7a-i**. Reagents and conditions: (a) acryloyl chloride, NaHCO_3 , CH_3CN , rt, 0.5 h, 95%; (b) $\text{Fe-NH}_4\text{Cl}$, $\text{MeOH-H}_2\text{O}$, 2 h, 70 °C, 72%; (c) ArNH_2 , DIPEA, 1,4-dioxane, 60°C, 2 h, 91%; (d) trifluoroacetic acid, intermediates **12a-h**, 2-BuOH, 100 °C, 12 h, 31% to 45%.



Scheme 2. Synthetic route of intermediates **12a,b**. Reagents and conditions: (a) K_2CO_3 , CH_3CN , 80 °C, 12 h, 63-85%; (b) $\text{Fe-NH}_4\text{Cl}$, $\text{MeOH-H}_2\text{O}$, 2 h, 70 °C, 60-87%.



Scheme 3. Synthetic route of intermediates **12c-e**. Reagents and conditions: (a) bromoacetyl bromide, NaHCO_3 , CH_3CN , rt, 0.5 h, 93%; (b) bis(2-methoxyethyl)amine, K_2CO_3 , CH_3CN , 80 °C, 12 h, 71-88%; (c) $\text{Fe-NH}_4\text{Cl}$, $\text{MeOH-H}_2\text{O}$, 2 h, 70 °C, 63-82%.



Scheme 4. Synthetic route of intermediates **12f-h**. Reagents and conditions: (a) ethyl bromoacetate, K_2CO_3 , CH_3CN , rt, 5 h, 91%; (b) KOH , $\text{MeOH-H}_2\text{O}$, 50 °C, 1 h, 62-78%; (c) $(\text{COCl})_2$, 50 °C, 1 h; (d) K_2CO_3 , CH_3CN , 80 °C, 12 h, 55-78%; (e) $\text{Fe-NH}_4\text{Cl}$, $\text{MeOH-H}_2\text{O}$, 2 h, 70 °C, 61-72%.

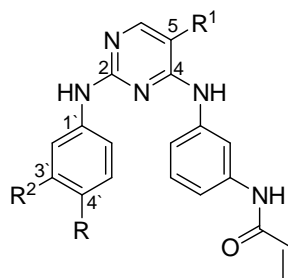
2.2. Biological activity

All these compounds were evaluated for their activity against BTK enzyme using ADP-Glo™ Kinase Assay [25-27]. Cell viability was determined by CCK-8 assay [18], and the cell cycle and apoptosis were analyzed by flow cytometer. Two typical B-cell lymphoblastic leukemia cell lines, Ramos and Raji, which overexpressed BTK enzyme, were used for the cell proliferation evaluations. For comparison, two novel

BTK inhibitors, ibrutinib and spebrutinib were also tested as reference compounds.

All these result data are depicted in Table 1.

Table 1 Biological activity of the newly synthesized DPPYs.^a



7a-l

Compound	5-R ¹	3'-R ²	4'-R	Enzymatic activity (IC ₅₀ , nM)		Antiproliferative activity (IC ₅₀ , μM) ^b	
				BTK	Ramos	Raji	
7a	Cl	H		4.94	13.0	30.5	
7b	F	H		7.12	18.1	23.8	
7c	Cl	H		2.83	18.1	20.1	
7d	F	H		27.2	>40.0	36.0	
7e	Cl	Cl		>100	16.9	19.3	
7f	Cl	H		22.6	14.8	19.9	
7g	F	H		91.3	35.6	36.9	
7h	Cl	OMe		>100	11.0	20.9	
7i	Cl	Me		20.0	19.6	35.6	
7j	Cl	H		12.1	10.5	19.1	
7k	F	H		22.4	22.3	38.6	
7l	Cl	H		0.23	>40	9.4	
Spebrutinib				0.72	20.9	29.4	

Ibrutinib

0.34

12.6

19.3

^aData represent the mean of at least three separate experiments. ^bDose-response curves were determined at five concentrations. The IC₅₀ values are the concentrations in micromolar needed to inhibit cell growth by 50% as calculated using GraphPad Prism version 5.0.

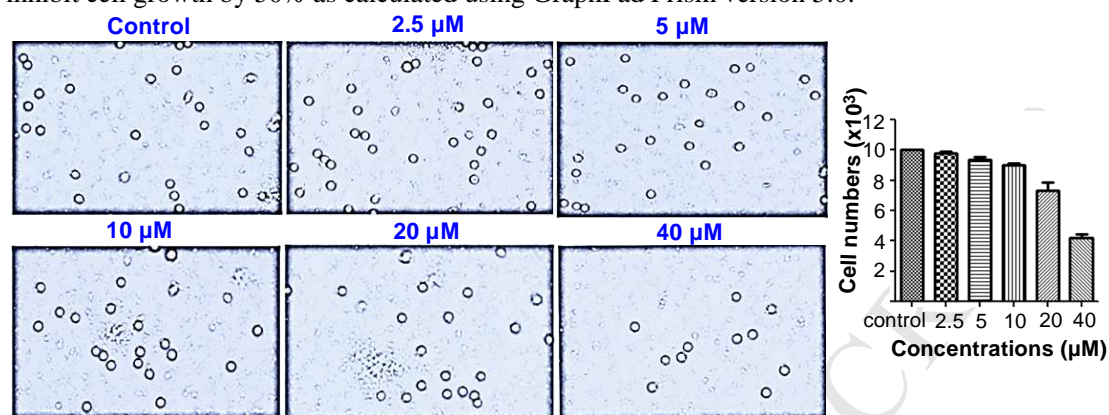


Fig. 4. Morphological changes of the PBMC cells treated by molecule **7j** (100 ×, final magnification) at concentration of 2.5, 5, 10, 20, 40 μM for 24 h. Cell numbers were calculated by traditional manual method with an ordinary cell counting chamber. One representative experiment is shown.

As for the kinase-based evaluation results shown in Table 1, these compounds effectively inhibit BTK enzyme at the concentrations less than 100 nmol/L, and four of them (**7a-c**, **7l**) displayed strong anti-BTK activity with IC₅₀ values lower than 7.12 nM. In particular, compound **7l** with IC₅₀ of 0.23 nM, is more potent than ibrutinib (IC₅₀ = 0.34 nM) and spebrutinib (IC₅₀ = 0.72 nM). SAR analysis revealed that substituents, such as chloro (**7e**), methoxy (**7h**), methyl (**7i**), were inappropriate to be installed on the C-3' position of the C-2 aniline side chain. Chloro substituent at the C-5 position of pyrimidine core is more favorable than the fluoro atom. Prolonging the C-2 aniline side chain is beneficial. The example analogues **7c** and **7l** bearing a long side chain possess very low effective inhibitory concentrations, with IC₅₀ values of 2.83 nM and 0.23 nM, respectively.

To confirm whether compound **7j** forms irreversible inhibition or not with BTK enzyme, the kinase activity determined by the luminescence value was detected after treating the inhibitor-linked BTK with the ADP-Glo™ Kinase Assay system (Table 2). Compared with the normal BTK (luminescence value = 9976), the inhibitor-linked

BTK made the luminescence value (383) significantly reduced, which indirectly proved that compound **7j** irreversibly contacts with BTK target, and thus led to the remarkable loss of the kinase activity.

Table 2 The luminescence values produced by treating BTK, and inhibitor-linked BTK with ADP-Glo™ Kinase Assay system.

	Times	Control ^a	Normal BTK ^b	Inhibitor-linked BTK ^c
Luminescence values	1	166	9702	430
	2	180	10652	412
	3	208	9574	308
	Ave.	185	9976	383

^a3 μ L 1 \times buffer, 2 μ L (0.5 μ g/ μ L substrate, 125 μ M ATP); ^b1 μ L 1 \times buffer, 2 μ L (0.5 μ g/ μ L substrate, 125 μ M ATP), 2 μ L 2.5 ng/ μ L enzyme; ^c1 μ L 500 nmol/L drug, 2 μ L (0.5 μ g/ μ L substrate, 125 μ M ATP), 2 μ L 2.5 ng/ μ L enzyme.

In cell-based assays, a large part of these molecules strongly inhibit the proliferations of Ramos and Raji cells at concentrations ranging from 10 to 20 μ mol/L. Inhibitor **7j**, possessing an IC₅₀ value of 12.1 nM in kinase-based activity, exhibited slightly stronger inhibitory activity against Ramos (IC₅₀ = 10.5 μ M) and Raji (IC₅₀ = 19.1 μ M) cells than reference compounds. Interestingly, molecule **7l**, the strongest inhibitor within these newly obtained DPPYs, could remarkably inhibit Raji cell line (IC₅₀ = 9.4 μ M), but was not sensitive to Ramos cells (IC₅₀ > 40 μ M). The analogues **7e** and **7h** also showed strong activity against the two B lymphoma cell lines, but they showed high IC₅₀ values (>100 nM) for targeting BTK kinase, suggesting that a new action mechanism for them to be produced to interfere with B-cell lymphoblastic leukemia cells. Fortunately, compound **7j** is not active to interfere with the normal PBMC cells at concentrations of less than 20 μ M, suggesting low cell cytotoxicity (Fig. 4). Overall, these biological explorations provided a new series of pyrimidine derivatives to inhibit B-cell lymphoblastic leukemia cells by targeting BTK.

2.3. Flow cytometry

In addition, to further investigate the antiproliferative mechanism of these inhibitors on B-cell leukemia cells, the most active inhibitor **7j**, was also examined

the effects on apoptosis and on the cell cycle in Ramos cell line using flow cytometry analysis [28,29]. For comparison, spebrutinib and ibrutinib were also evaluated as the reference compounds. As shown in Fig. 5, inhibitor **7j** could significantly induce the Ramos cells apoptosis, and the apoptosis rates were 38.0%, 46.8% and 83.6% at concentrations of 5 $\mu\text{mol/L}$, 10 $\mu\text{mol/L}$, and 20 $\mu\text{mol/L}$ inhibitor **7j**, respectively. Compared to spebrutinib (41.5%) and ibrutinib (47.9%), **7j** could inhibit the proliferations of Ramos cell line and induce the similar cell apoptosis rates at the low concentrations of 10 $\mu\text{mol/L}$. After incubation with 5 $\mu\text{mol/L}$, 10 $\mu\text{mol/L}$ and 20 $\mu\text{mol/L}$ inhibitor **7j** for 48h, the DNA contents of the Ramos cells were 53.18%, 63.1% and 70.8% in G₀/G₁ phase, and were 46.8%, 37.0% and 28.4% in S phase, respectively (Fig. 6). Apparently, the newly synthesized molecule **7j** blocked Ramos cells at the G₀/G₁ phase, while ibrutinib (G₂ phase) and spebrutinib (S phase) arrested the cell cycle at the late phase.

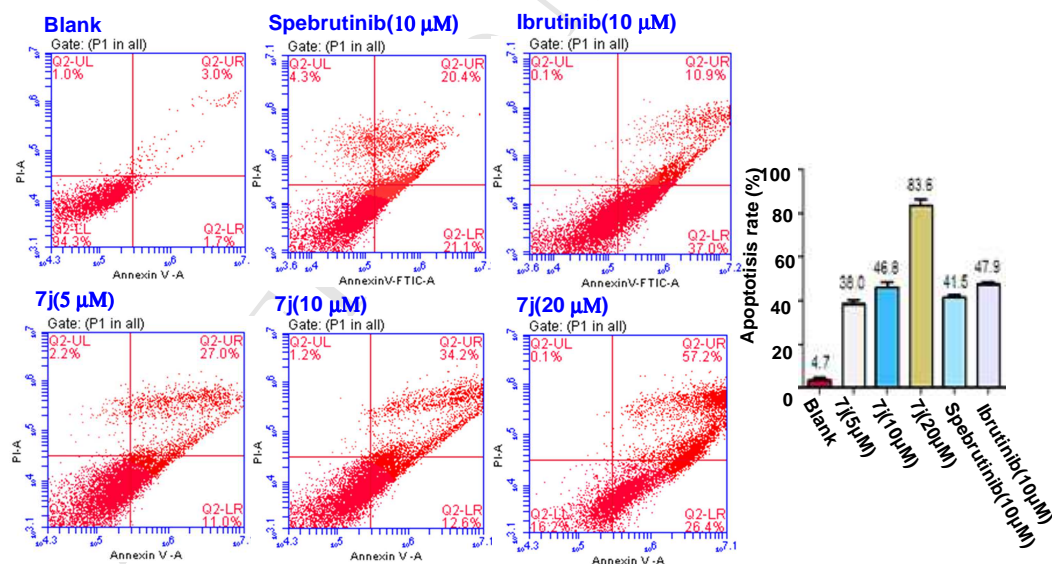


Fig. 5. Compound **7j** induced Ramos cell apoptosis *in vitro*. The cells were incubated with the indicated concentrations of **7j** for 48 h, and the cells were stained with annexin V/FTIC, followed by flow cytometry analysis. One representative experiment is shown. $p < 0.05$.

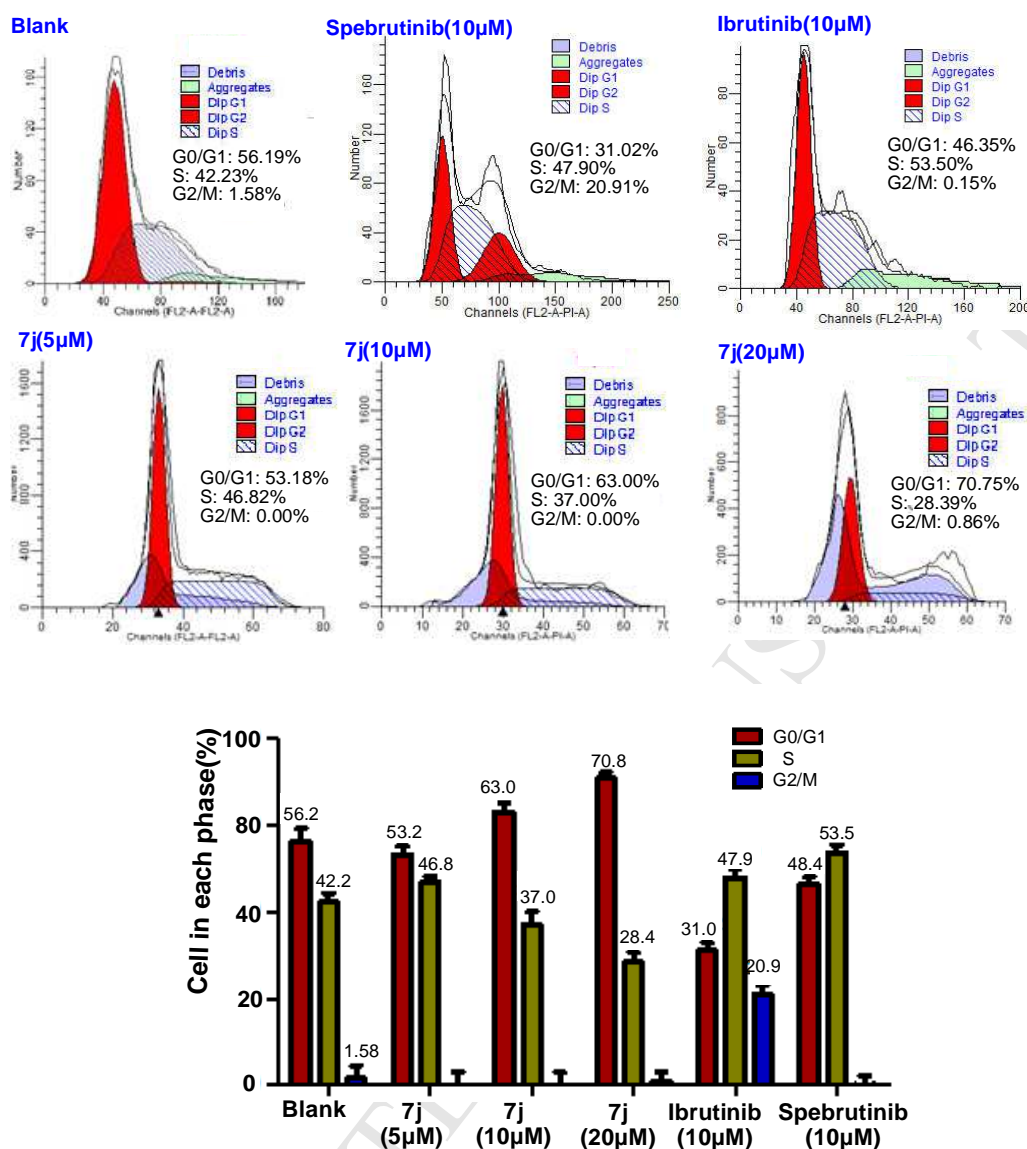


Fig. 6. Effects of spebrutinib, ibrutinib and 7j on Ramos cell cycle arrest detected by flow cytometry assay. Results are representative of three separate experiments, dates are expressed as the mean \pm standard deviation, $p < 0.05$.

2.4. Molecular modeling calculations

In order to investigate the interaction mechanism of the newly synthesized DPPYs with BTK enzyme, three potent BTK inhibitors **7a**, **7c**, **7l**, and two less active inhibitors **7e**, **7h**, in parallel with the lead compound spebrutinib were docked into the ATP binding pocket of BTK enzyme (PDB: 3GEN), respectively [30]. The program AutoDock 4.2 with its default parameters were used [31-33]. The molecular simulations were depicted in Fig. 7. By analyzing the binding model of spebrutinib

with BTK (Fig. 7a), it was found that several important interaction forces were produced, including: (1) covalent bond forces between the essential acrylamide functionality of spebrutinib with the amino acid Cys481; (2) Hydrogen-bond interactions formed by the carbonyl group of acrylamide substituent with the amino acid Lys430 through a water molecule; (3) strong contacts between the C-2 aniline side chain of pyrimidine core with Ser538, Phe540, Ile472, which consist of the bottom section of the ATP binding pocket; (4) hydrophobic interactions generated from the C-5 chlorine atom of pyrimidine core with the mutant gatekeeper residue Met477. Compared with spebrutinib, the three potent inhibitors **7a** (Fig. 7b), **7c** (Fig. 7d) and **7l** (Fig. 7c), retained the important covalent bond formed by the acrylamide substituent with Cys481. But the less active inhibitors **7e** (Fig. 7e) and **7h** (Fig. 7f) lost these important interactions. Beyond the hydrogen bond between the carbonyl group in acrylamide functionality with Lys430, compounds **7a**, **7c** and **7l**, produced additional strong hydrogen-bond contacts, including forces between oxygen atom in C-2 aniline side chain of **7a** with Phe540 through a water molecule, forces between the carbonyl group in C-2 aniline side chain of **7c** with Lys430 through a water molecule, and forces between carbonyl group in C-2 aniline side chain with Ser538. Clearly, **7a** firmly occupied the ATP-binding pocket, maintaining the strong interactions generated from the C-5 chlorine atom of pyrimidine ring with the residue Met477. In terms of compounds **7c** and **7l**, the pyrimidine core was squeezed out of the pocket, and directly reaches into the residue Asn484, thus forming new supplementary binding forces. In contrast, the less active inhibitors **7e** and **7h** almost lost these important interactions, and thus were not effective to interfere with BTK. Overall, these binding modes actually explained their activity data.

3. Conclusion

A new series of DPPYs bearing various aniline side chains at the C-2 position of pyrimidine core were synthesized as potent BTK inhibitors. Most of them exhibited equivalent capacity as lead compound (spebrutinib and ibrutinib) in both kinase-based and cell-based assays. It was significant that the most active inhibitor **7i**, which were able to interfere with BTK kinase at concentrations of 0.23 nM, was discovered in this contribution. Notably, the novel molecule **7j** with IC₅₀ values of 10.5 μM against Ramos cells and 19.1 μM against Raji cells, showed stronger activity than the available BTK inhibitors (spebrutinib and ibrutinib). In conclusion, these findings expanded the structural diversity of pyrimidine derivatives as irreversible inhibitors of BTK, and provided new insight to discover more effective BTK inhibitors.

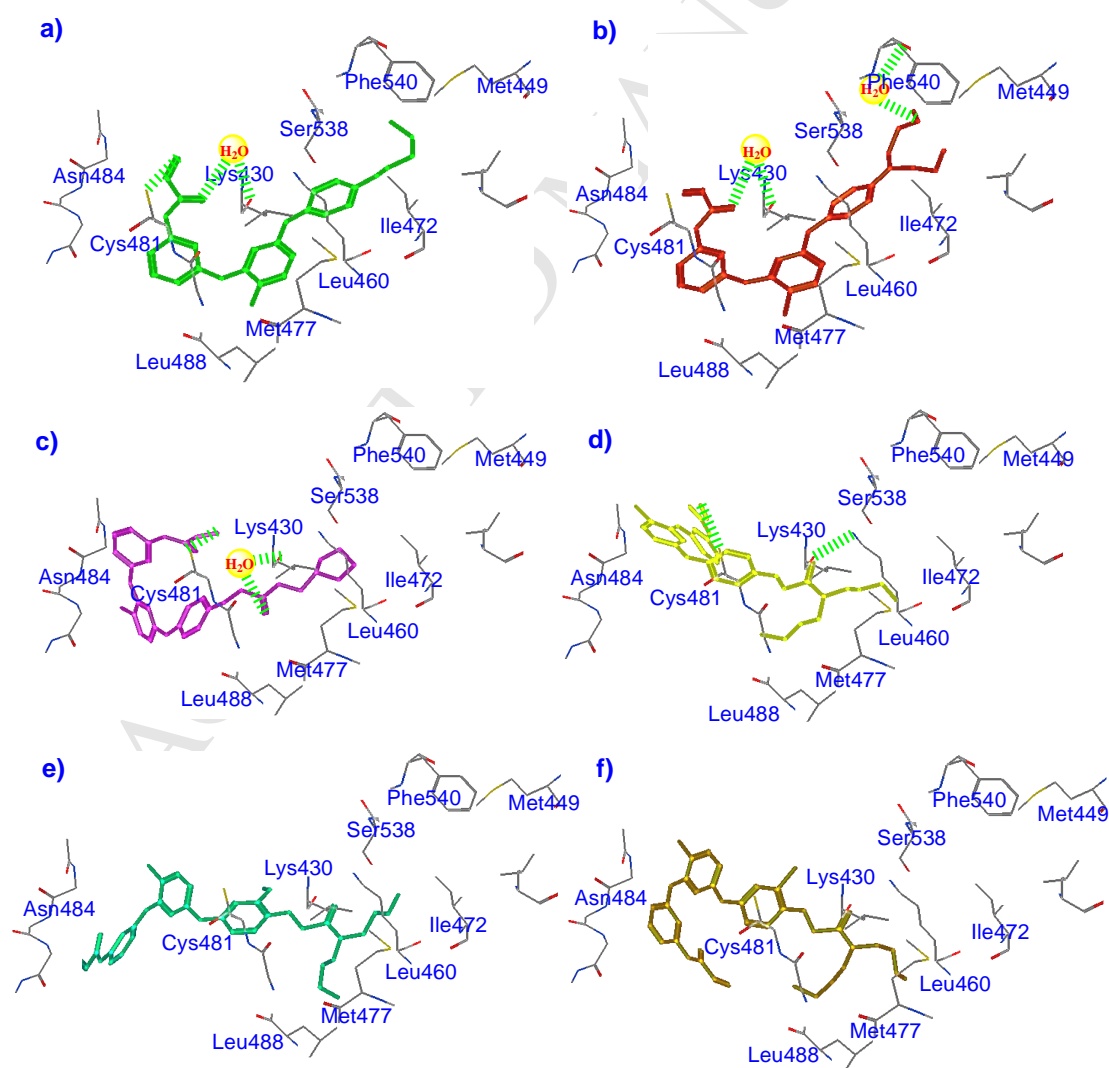


Fig. 7. a) Putative binding mode of spebrutinib within BTK (PDB code: 3GEN); b) Putative binding mode of inhibitor **7a** within BTK (PDB code: 3GEN); c) Putative binding mode of inhibitor **7i** within BTK (PDB code: 3GEN); d) Putative binding mode of inhibitor **7c** within BTK (PDB code: 3GEN); e) Putative binding mode of inhibitor **7e** within BTK (PDB code: 3GEN); f) Putative binding mode of inhibitor **7h** within BTK (PDB code: 3GEN).

4. Experimental section

4.1. General Methods and Chemistry

Solvents and reagents were obtained from commercial supplies and were used without further purification. High resolution ESI-MS were performed on an AB Sciex TripleTOF[®] 4600 LC/MS/MS system. ¹H NMR and ¹³C NMR spectra on a Bruker AV 400 MHz spectrometer were recorded in [*d*]DMSO. Coupling constants (*J*) are expressed in hertz (Hz). Chemical shifts (δ) of NMR are reported in parts per million (ppm) units relative to internal control (TMS). All reactions were monitored by TLC, using silica gel plates with fluorescence F254 and UV light visualization. Flash chromatography separations were obtained on Silica Gel (300–400 mesh) using dichloromethane/methanol as eluents.

4.2. General procedure for the synthesis of **7a–l** [21-24]

4-Morpholine-substituted aniline intermediates **12a–h** were prepared according to the literatures 23 and 24. While the intermediates *N*-(3-((2-chloro-5-substitutedpyrimidin-4-yl)oxy)phenyl)acrylamides **11a–b** were synthesized using the procedures reported in references 21 and 22. All these intermediates were directly used without any purification and structural characterization. With these intermediates in hand, the newly obtained compounds were synthesized as described below.

A flask was charged with compounds **11a–b** (0.70 mmol), **12a–h** (0.70 mmol), TFA (0.08 mL, 1.05 mmol), and 2-BuOH (10 mL). The slurry was heated to 100 °C for 12 h. Then, the reaction mixture was allowed to cool to room temperature and was neutralized with a saturated aqueous sodium bicarbonate solution. The aqueous

mixture was extracted with CH₂Cl₂ three times (20 mL × 3). The crude product was purified using flash chromatography with dichloromethane/methanol (v/v, 1:1) as eluents.

4.2.1. N-(3-((5-Chloro-2-(4-(bis(2-methoxyethyl)amino))phenylamino-4-pyrimidinyl)amino)phenyl)acrylamide (7a). Yield: 15.50%; off-yellow solid; ¹H NMR (400MHz, DMSO-*d*₆): δ 3.21 (s, 6H), 3.38 (s, 8H), 5.73 (dd, *J* = 4.0 Hz, 8.0 Hz, 1H), 6.24 (dd, *J* = 4.0 Hz, 16.0 Hz, 1H), 6.44 (dd, *J* = 8.0 Hz, 16.0 Hz, 3H), 7.21–7.31 (m, 4H), 7.46 (d, *J* = 4.0 Hz, 1H), 7.85 (s, 1H), 8.02 (s, 1H), 8.76 (s, 1H), 8.89 (s, 1H), 10.14 (s, 1H); ¹³CNMR (400 MHz, DMSO-*d*₆): δ 50.65 (2C), 58.63 (2C), 70.13 (2C), 103.00, 111.89 (2C), 115.19, 115.43, 119.22, 121.84 (2C), 127.31, 128.87, 129.76, 132.28, 139.38, 139.43, 143.42, 155.15, 156.36, 158.44, 163.48; HRMS (ESI) for C₂₅H₂₉ClN₆O₃, (M+H)⁺ calcd: 497.2062; found: 497.2044.

4.2.2. N-(3-((5-Fluorine-2-(4-(bis(2-methoxyethyl)amino))phenylamino-4-pyrimidinyl)amino)phenyl)acrylamide (7b). Yield: 12.34%; off-yellow solid; ¹H NMR (400MHz, DMSO-*d*₆): δ 3.34 (s, 6H), 3.42 (s, 8H), 5.75 (dd, *J* = 4.0 Hz, 8.0 Hz, 1H), 6.25 (dd, *J* = 4.0 Hz, 16.0 Hz, 1H), 6.44–6.55 (m, 3H), 7.19–7.42 (m, 4H), 7.51(d, *J* = 8.0 Hz, 1H), 7.95 (s, 1H), 8.01 (d, *J* = 4.0 Hz, 1H), 8.75 (s, 1H), 9.31 (s, 1H), 10.15 (s, 1H); ¹³C NMR (400 MHz, DMSO-*d*₆): δ 51.01 (2C), 58.94 (2C), 70.46 (2C), 112.36 (2C), 113.73, 115.12, 117.79, 122.01 (2C), 127.59, 129.28, 130.67, 132.63, 139.61, 139.76, 139.95 (*J* = 76.0 Hz), 141.46, 141.65 (*J* = 76.0 Hz), 142.05, 143.62, 150.28, 150.39 (*J* = 44.0 Hz), 156.78, 163.79; HRMS (ESI) for C₂₅H₂₉FN₆O₃, (M+H)⁺ calcd: 481.2358; found: 480.2279.

4.2.3. N-(3-((5-Chloro-2-(4-(2-(bis(2-methoxyethyl)amino)-2-oxoethoxy)phenylamino)-4-pyrimidinyl)amino)phenyl)acrylamide (7c). Yield: 14.72%; off-brown solid; ¹H NMR (400 MHz, DMSO-*d*₆): δ 3.24 (s, 3H), 3.29 (s, 3H), 3.44 (dd, *J* = 8.0 Hz, 16.0 Hz, 4H), 3.51 (s, 4H), 4.75 (s, 2H), 5.75 (dd, *J* = 4.0 Hz, 8.0 Hz, 1H), 6.27 (dd, *J* = 4.0 Hz, 16.0 Hz, 1H), 6.47 (dd, *J* = 8.0 Hz, 16.0 Hz, 1H), 6.68 (d, *J* = 8.0 Hz, 2H), 7.28–7.49 (m, 5H), 7.87 (s, 1H), 8.10 (s, 1H), 8.89 (s, 1H), 9.13 (s, 1H), 10.19 (s, 1H); ¹³CNMR (400 MHz, DMSO-*d*₆): δ 44.88, 46.81, 58.09, 58.42, 69.67, 65.80, 70.10, 103.32, 114.08 (2C), 115.00, 115.32, 119.11, 120.62 (2C), 126.96, 128.54, 131.89, 133.69, 138.92, 139.06, 152.95, 154.79, 156.09, 157.83, 163.15, 167.79; HRMS (ESI) for C₂₇H₃₁ClN₆O₅, (M+H)⁺ calcd: 555.2117; found: 555.2105.

4.2.4. N-(3-((5-Fluoro-2-(4-(2-(bis(2-methoxyethyl)amino)-2-oxoethoxy)phenylamino)-4-pyrimidinyl)amino)phenyl)acrylamide (7d). Yield: 25.25%; off-brown solid; ¹H NMR (400 MHz, DMSO-*d*₆): δ 3.25 (s, 3H), 3.30(s, 3H), 3.45 (dd, *J* = 4.0 Hz, 16.0 Hz, 4H), 3.52–3.53 (br, 4H), 4.78 (s, 2H), 5.78 (dd, *J* = 4.0

Hz, 8.0 Hz, 1H), 6.29 (dd, $J = 4.0$ Hz, 16.0 Hz, 1H), 6.49 (dd, $J = 8.0$ Hz, 16.0 Hz, 1H), 6.75 (d, $J = 8.0$ Hz, 2H), 7.29 (t, $J = 8.0$ Hz, 1H), 7.43 (d, $J = 8.0$ Hz, 1H), 7.53 (d, $J = 8.0$ Hz, 2H), 7.58 (d, $J = 8.0$ Hz, 1H), 7.94 (s, 1H), 8.08 (d, $J = 4.0$ Hz, 1H), 8.99 (s, 1H), 9.41 (s, 1H), 10.16 (s, 1H); ^{13}C NMR (400 MHz, DMSO- d_6): δ 45.25, 47.19, 58.47, 58.80, 66.23, 70.05, 70.48, 113.50, 114.53 (2C), 115.01, 117.64, 120.73 (2C), 127.27, 129.00, 132.31, 134.58, 139.45, 139.54 ($J = 36.0$ Hz), 141.07, 141.26 ($J = 76.0$ Hz), 141.98, 150.05, 150.16 ($J = 44.0$ Hz), 153.17, 156.11, 156.13, 163.49, 168.22; HRMS (ESI) for $\text{C}_{27}\text{H}_{31}\text{FN}_6\text{O}_5$, (M+H) $^+$ calcd: 539.2413; found: 539.2407.

4.2.5. *N*-(3-((5-Chloro-2-(3-chloro-4-(2-(bis(2-methoxyethyl)amino)-2-oxoethoxy)-phenylamino)-4-pyrimidinyl)amino)phenyl)acrylamide (7e). Yield: 16.96%; off-yellow solid; ^1H NMR (400 MHz, DMSO- d_6): δ 3.25 (s, 3H), 3.30 (s, 3H), 3.45 (dd, $J = 4.0$ Hz, 16.0 Hz, 4H), 3.53 (s, 4H), 4.89 (s, 2H), 5.77 (dd, $J = 4.0$ Hz, 8.0 Hz, 1H), 6.27 (dd, $J = 4.0$ Hz, 16.0 Hz, 1H), 6.47 (dd, $J = 8.0$ Hz, 16.0 Hz, 1H), 6.77 (d, $J = 9.0$ Hz, 1H), 7.32 (t, $J = 8.0$ Hz, 1H), 7.39 (dd, $J = 4.0$ Hz, 8.0 Hz, 2H), 7.50 (d, $J = 8.0$ Hz, 1H), 7.77 (s, 1H), 7.86 (s, 1H), 8.16 (s, 1H), 8.95 (s, 1H), 9.30 (s, 1H), 10.19 (s, 1H); ^{13}C NMR (400 MHz, DMSO- d_6): δ 45.25, 47.16, 58.48, 58.80, 66.75, 70.02, 70.41, 104.34, 113.99, 115.13, 115.78, 118.84, 119.37, 120.72, 121.05, 127.27, 129.14, 132.32, 134.84, 139.19, 139.65, 148.52, 155.11, 156.50, 157.93, 163.52, 167.70; HRMS (ESI) for $\text{C}_{27}\text{H}_{30}\text{Cl}_2\text{N}_6\text{O}_5$, (M+H) $^+$ calcd: 589.1727, found: 589.1714.

4.2.6. *N*-(3-((5-Chloro-2-(4-(2-(bis(2-methoxyethyl)amino)acetyl)amino)phenylamino)-4-pyrimidinyl)amino)phenyl)acrylamide (7f). Yield: 13.89%; off-yellow solid; ^1H NMR (400 MHz, DMSO- d_6): δ 2.79 (t, $J = 4.0$ Hz, 4H), 3.26 (s, 8H), 3.43 (t, $J = 4.0$ Hz, 4H), 5.77 (dd, $J = 4.0$ Hz, 8.0 Hz, 1H), 6.25-6.31 (m, 1H), 6.45-6.51 (m, 1H), 7.26-7.43 (m, 4H), 7.54 (dd, $J = 8.0$ Hz, 16.0 Hz, 3H), 7.90 (s, 1H), 8.15 (s, 1H), 8.95 (s, 1H), 9.30 (s, 1H), 9.64 (s, 1H), 10.21 (s, 1H); ^{13}C NMR (400 MHz, DMSO- d_6): δ 54.74 (2C), 58.51 (2C), 59.36, 70.56 (2C), 103.97, 110.81, 115.02, 115.35, 115.63, 119.24, 119.60, 127.23, 128.86, 129.42, 132.28, 132.72, 136.38, 139.29, 139.59, 155.14, 156.54, 158.03, 163.54, 169.55; HRMS (ESI) for $\text{C}_{27}\text{H}_{32}\text{ClN}_7\text{O}_4$, (M+H) $^+$ calcd: 554.2277; found: 554.2269.

4.2.7. *N*-(3-((5-Fluoro-2-(4-(2-(bis(2-methoxyethyl)amino)acetyl)amino)phenylamino)-4-pyrimidinyl)amino)phenyl)acrylamide (7g). Yield: 15.5%; off-yellow solid; ^1H NMR (400 MHz, DMSO- d_6): δ 2.77 (t, $J = 8.0$ Hz, 4H), 3.25 (s, 8H), 3.42 (t, $J = 4.0$ Hz, 4H), 5.75 (dd, $J = 4.0$ Hz, 8.0 Hz, 1H), 6.26 (dd, $J = 4.0$ Hz, 16.0 Hz, 1H), 6.47 (dd, $J = 8.0$ Hz, 16.0 Hz, 1H), 7.28 (t, $J = 8.0$ Hz, 1H), 7.39 (d, $J = 8.0$ Hz, 2H), 7.44 (d, $J = 8.0$ Hz, 1H), 7.55 (d, $J = 8.0$ Hz, 1H), 7.61 (d, $J = 8.0$ Hz, 2H), 7.95 (s, 1H), 8.10 (d, $J = 4.0$ Hz, 1H), 9.14 (s, 1H), 9.43 (s, 1H), 9.63 (s, 1H), 10.17 (s, 1H); ^{13}C

NMR (400 MHz, DMSO-*d*₆): δ 54.81 (2C), 58.58 (2C), 59.43, 70.65 (2C), 113.59, 115.05, 117.85, 119.37 (2C), 119.39, 127.26, 129.04, 132.40, 132.56, 136.95, 139.58, 139.65 (*J* = 28.0 Hz), 139.70, 141.11, 141.30 (*J* = 76.0 Hz), 142.15, 150.17, 150.28 (*J* = 44.0 Hz), 155.94, 155.97, 163.60, 169.59; HRMS (ESI) for C₂₇H₃₂FN₇O₄, (M+H)⁺ calcd: 538.2573; found: 538.2563.

4.2.8. *N*-(3-((5-Chloro-2-(3-methoxy-4-(2-(bis(2-methoxyethyl)amino)acetylamino)phenylamino)-4-pyrimidinyl)amino)phenyl)acrylamide (**7h**). Yield: 10.2%; off-yellow solid; ¹H NMR (400 MHz, DMSO-*d*₆): δ 2.81 (t, *J* = 4.0 Hz, 4H), 3.24-3.28 (m, 8H), 3.47 (t, *J* = 4.0 Hz, 4H), 3.65 (s, 3H), 5.79 (dd, *J* = 4.0 Hz, 8.0 Hz, 1H), 6.29 (dd, *J* = 4.0 Hz, 16.0 Hz, 1H), 6.49 (dd, *J* = 8.0 Hz, 16.0 Hz, 1H), 7.24 (d, *J* = 9.0 Hz, 1H), 7.32 (t, *J* = 8.0 Hz, 1H), 7.43 (d, *J* = 8.0 Hz, 2H), 7.52 (d, *J* = 8.0 Hz, 1H), 7.91 (s, 1H), 8.03 (d, *J* = 9.0 Hz, 1H), 8.20 (s, 1H), 8.97 (s, 1H), 9.30 (s, 1H), 9.60 (s, 1H), 10.20 (s, 1H); ¹³C NMR (400 MHz, DMSO-*d*₆): δ 55.23 (2C), 55.83, 58.43 (2C), 60.44, 71.00 (2C), 102.86, 104.27, 110.96, 115.06, 115.60, 119.36, 121.67, 127.20, 128.93, 132.28, 136.92, 139.34, 139.62, 148.47, 148.72, 155.11, 156.39, 158.06, 163.50, 169.16; HRMS (ESI) for C₂₈H₃₄ClN₇O₅, (M+H)⁺ calcd: 584.2383, found: 584.2379.

4.2.9. *N*-(3-((5-Chloro-2-(3-methyl-4-(2-(bis(2-methoxyethyl)amino)acetylamino)phenylamino)-4-pyrimidinyl)amino)phenyl)acrylamide (**7i**). Yield: 18.80%; off-brown solid; ¹H NMR (400 MHz, DMSO-*d*₆): δ 2.05 (s, 3H), 2.76 (t, *J* = 4 Hz, 4H), 3.17 (s, 6H), 3.23 (s, 2H), 3.41 (t, *J* = 4.0 Hz, 4H), 5.73 (dd, *J* = 4.0 Hz, 8.0 Hz, 1H), 6.23 (dd, *J* = 4.0 Hz, 16.0 Hz, 1H), 6.43 (dd, *J* = 9.0 Hz, 16.0 Hz, 1H), 7.31 (d, *J* = 8.0 Hz, 3H), 7.52 (d, *J* = 8.0 Hz, 2H), 7.65 (d, *J* = 8.0 Hz, 1H), 7.85 (s, 1H), 8.13 (s, 1H), 8.91 (s, 1H), 9.23 (s, 1H), 9.38 (s, 1H), 10.18 (s, 1H); ¹³C NMR (400 MHz, DMSO-*d*₆): δ 55.17 (2C), 58.38 (3C), 59.67, 70.65 (2C), 103.92, 115.33, 115.64, 117.10, 119.63, 120.72, 121.70, 127.22, 128.85, 129.05, 130.50, 132.27, 136.91, 139.34, 139.66, 155.16, 156.53, 158.08, 163.51, 169.43; HRMS (ESI) for C₂₈H₃₄ClN₇O₄, (M+H)⁺ calcd: 568.2434; found: 568.2410.

4.2.10. *N*-(3-((5-Chloro-2-(4-((tetrahydro-2-furanyl)methoxy)phenylamino)-4-pyrimidinyl)amino)phenyl)acrylamide (**7j**). Yield: 16.56%; off-white solid; ¹H NMR (400 MHz, DMSO-*d*₆): δ 1.61–1.68 (m, 1H), 1.81–1.90 (m, 2H), 1.95–2.01 (m, 1H), 3.67–3.70 (m, 1H), 3.75–3.82 (m, 3H), 4.09–4.12 (m, 1H), 5.75 (dd, *J* = 4.0 Hz, 8.0 Hz, 1H), 6.27 (dd, *J* = 4.0 Hz, 16.0 Hz, 1H), 6.47 (dd, *J* = 8.0 Hz, 16.0 Hz, 1H), 6.70 (d, *J* = 8.0 Hz, 2H), 7.32 (t, *J* = 8.0 Hz, 2H), 7.50 (t, *J* = 8.0 Hz, 3H), 7.90 (s, 1H), 8.11 (s, 1H), 8.91 (s, 1H), 9.17 (s, 1H), 10.22 (s, 1H); ¹³C NMR (400 MHz, DMSO-*d*₆): δ 25.59, 28.13, 67.83, 70.61, 76.91, 103.58, 114.40 (2C), 115.68, 115.82, 119.53, 120.85 (2C), 127.33, 128.99, 132.26, 133.99, 139.25, 139.41, 153.66, 155.19,

156.51, 158.15, 163.51; HRMS (ESI) for $C_{24}H_{24}ClN_5O_3$, $(M+H)^+$ calcd: 466.1640; found: 466.1630.

4.2.11. *N*-(3-((5-Fluoro-2-(4-((tetrahydro-2-furanyl)methoxy)phenylamino)-4-pyrimidinyl)amino)phenyl)acrylamide (**7k**). Yield: 12.80%; off-white solid; 1H NMR (400 MHz, DMSO- d_6): δ 1.54–1.63 (m, 1H), 1.76–1.84 (m, 2H), 1.89–1.97 (m, 1H), 3.59–3.64 (m, 1H), 3.69–3.78 (m, 3H), 4.03–4.09 (m, 1H), 5.70 (dd, $J = 4.0$ Hz, 16.0 Hz, 1H), 6.21 (dd, $J = 4.0$ Hz, 16.0 Hz, 1H), 6.42 (dd, $J = 8.0$ Hz, 16 Hz, 1H), 6.70 (d, $J = 9.0$ Hz, 2H), 7.23 (t, $J = 8.0$ Hz, 1H), 7.40 (dd, $J = 8.0$ Hz, 16.0 Hz, 2H), 7.48 (d, $J = 8.0$ Hz, 2H), 7.91 (s, 1H), 8.02 (d, $J = 4.0$ Hz, 1H), 8.95 (s, 1H), 9.34 (s, 1H), 10.12 (s, 1H); ^{13}C NMR(400 MHz, DMSO- d_6): δ 26.20, 28.73, 68.43, 71.25, 77.54, 114.41, 115.09 (2C), 115.75, 118.32, 121.20 (2C), 127.88, 129.66, 132.90, 135.09, 140.02, 140.07 ($J = 20.0$ Hz), 141.71, 141.90 ($J = 76.0$ Hz), 142.53, 150.67, 150.78 ($J = 44.0$ Hz), 154.10, 156.65, 156.68, 164.09; HRMS (ESI) for $C_{24}H_{24}FN_5O_3$, $(M+H)^+$ calcd: 450.1936; found: 450.1932.

4.2.12. (Tetrahydro-2-furanyl)methyl,2-(4-((5-chloro-4-((3-((1-oxo-2-propen-1-yl)amino)phenyl)amino)-2-pyrimidinyl)amino)phenoxy)acetate (**7l**). Yield: 12.86%; off-yellow solid; 1H NMR (400 MHz, DMSO- d_6): δ 1.49–1.56 (m, 4H), 3.68 (d, $J = 8.0$ Hz, 1H), 4.58 (d, $J = 4.0$ Hz, 1H), 4.61–4.66 (m, 3H), 4.79–4.84 (m, 2H), 5.24 (s, 1H), 6.53 (d, $J = 8.0$ Hz, 2H), 6.71 (dd, $J = 4.0$ Hz, 8.0 Hz, 2H), 7.27 (dd, $J = 8.0$ Hz, 16.0 Hz, 2H), 7.49 (d, $J = 8.0$ Hz, 3H), 7.80 (s, 1H), 8.09 (s, 1H), 8.87 (s, 1H), 9.17 (s, 1H), 9.99 (s, 1H); ^{13}C NMR(400 MHz, DMSO- d_6): δ 19.96, 28.88, 65.69, 66.29, 73.12, 73.27, 104.06, 113.75, 114.84, 116.25, 121.04, 127.66, 129.09, 132.54, 134.90, 139.49, 139.56, 139.74, 139.96, 144.13, 149.81, 152.97, 155.41, 156.82, 158.41, 163.83; HRMS (ESI) for $C_{26}H_{26}ClN_5O_5$, $(M+H)^+$ calcd: 524.1695; found: 524.1684.

4.3 Biological evaluation

4.3.1 Cell culture and reagents

Ramos and Raji cells were purchased from Fuheng Biology Company (Shanghai, China). Peripheral blood mononuclear (PBMC) cells were obtained from a healthy adult male. The Cell Counting Kit-8 (CCK-8) reagent was purchased from Biotool Company (Switzerland). The BTK enzyme and the ADP-Glo™ Kinase Assay system that measures ADP formed from a kinase reaction were purchased from Promega Corporation (USA). The Annexin V-FITC Apoptosis Detection Kit and Cell Cycle Assay were purchased from Beyotime Company (China). All cell lines were grown in RPMI-1640 (Gibco®, USA) supplemented with 10% FBS (Gibco®, USA), 1%

penicillin-streptomycin (Beyotime Company, China). The cells were maintained and propagated as monolayer cultures at 37 °C in humidified 5% CO₂ incubator.

4.3.2. *In vitro* kinase enzymatic assay

The BTK kinase enzyme system (Catalog. V9071) was purchased from Promega Corporation (USA). Concentrations consisting of suitable levels from 0.1 to 100 nM were used for all of the tested compounds. The experiments were performed according to the instructions of the manufacturer. The more detailed and complete protocols, see the ADP-Glo™ kinase Assay Technical Manual available at: <http://cn.promega.com/resources/protocols/product-information-sheets/n/btk-kinase-enzyme-system-protocol/>. The test was performed in a 384-well plate, and includes the major steps below: (1) perform a 5 μL kinase reaction using 1× kinase buffer (e.g., 1× reaction buffer A), (2) incubate at room temperature for 60 minutes, (3) add 5 μL of ADP-Glo™ Reagent to stop the kinase reaction and deplete the unconsumed ATP, leaving only ADP and a very low background of ATP, (4) incubate at room temperature for 40 minutes, (5) add 10 μL of Kinase Detection, (6) reagent to convert ADP to ATP and introduce luciferase and luciferin to detect ATP, (7) incubate at room temperature for 30 minutes, (8) plate was measured on TriStar® LB942 Multimode Microplate Reader (BERTHOLD) to detect the luminescence (Integration time 0.5-1 second). Curve fitting and data presentations were performed using GraphPad Prism version 5.0.²⁵⁻²⁷

The procedure to detect whether compound **7j** forms irreversible inhibition or not with BTK enzyme based on the ADP-Glo™ Kinase Assay system. Briefly, the procedure includes: 1) Add inhibitor **7j** (1 μL, 50 μmol/L) to 1×buffer (99 μL) to afford 100 μL drug solution (500 nmol/L); 2) Dilute enzyme (10 μL) with 1×buffer (190 μL) to provide 200 μL (2.5 ng/μL) enzyme solution; 3) Mix the drug solution (100 μL) and the diluted enzyme solution (200 μL) at room temperature for 60 min, then extract with dichloromethane two times (2×300 μL), the water solution containing the inhibitor-linked BTK was retained; 4) Add substrate (100 μL) and ATP (2.5 μL) to 1×buffer (97.5 μL) to afford the substrate/ATP mixture (200 μL); 5) Combine the substrate/ATP mixture (2 μL) prepared in step 4 with the BTK-

contained solution (3 μ L), then incubate at room temperature for 60 min; 6) Add 5 μ L of ADP-Glo™ Reagent, and incubate at room temperature for 40 minutes to stop the kinase reaction and deplete the unconsumed ATP; 6) Add 10 μ L of Kinase Detection, and incubate at room temperature for 30 minutes; 7) Record luminescence (Integration time 0.5-1 second).

4.3.3 Cellular activity assay

All the cell viability assays were performed according to the CCK-8 method. The cells were seeded in 96-well plates at a density of 2,000 to 3,000 cells/well and were maintained at 37 °C in a 5% CO₂ incubator in RPMI1640 containing 10% fetal bovine serum (FBS, Gibco) for one day. Cells were exposed to treatment for 48 h, and the number of cells used per experiment for each cell lines was adjusted to obtain an absorbance of 0.5 to 1.2 at 450 nm with a microplate reader (Thermo, USA). Compounds were tested at appropriate concentrations (1.25 to 40 μ M), with each concentration duplicated five times. The IC₅₀ values were calculated using GraphPad Prim version 5.0.

4.3.4 Cytotoxic activity assay

Peripheral venous blood was collected in an ACD anticoagulant (V_{blood}: V_{anticoagulant} = 9:1) tube from the normal healthy adult male. The leucocyte-rich plasma was removed and the peripheral blood mononuclear cells (PBMC) consisting of monocytes and the lymphocytes were separated on Lymphoprep (density 1.077g/ml, Nyegaard & Co. As., Oslo, Norway). The cells collected from the interface layer were washed three times with PBS buffered salt solution and counted using cell counting chamber.

PBMC cells were seeded in 24-well plates at a density of 8,000 to 10,000 cells/well. Cells were treated with inhibitor **7j** at appropriate concentrations (2.5, 5, 10, 20, 40 μ M), with each concentration duplicated five times. Aftering maintaining the cells at 37 °C in a 5% CO₂ incubator in RPMI1640 containing 10% fetal bovine serum (FBS, Gibco) for 24 h, the morphology of the cells was observed with a phase contrast microscope (Nikon, Japan), and the number of living PBMC cells was calculated by traditional manual method with an ordinary cell counting chamber.

4.3.5 Flow cytometry assay

The Ramos and Raji cells (1 to 5×10^5 cells/well) incubated in 6-well plates were treated with solvent control (DMSO), spebrutinib, ibrutinib, or compound **7j** in medium containing 5% FBS for 48 h. Then, collected and fixed with 70% ethanol at 4 °C overnight. After being fixed with 75% ethanol at 4 °C for 24 h, the cells were stained with Annexin V-FITC (5 μ L)/propidium iodide (5 μ L), and analyzed by flow cytometry assay (Becton-Dickinson, USA). For cell cycle analysis, Ramos and Raji cells at a density of approximately 2×10^5 cells/well were incubated in 6-well plates, treated with different concentrations of inhibitors for 48 h, collected and fixed with 70% ethanol at 4 °C overnight. After fixation, the cells were washed with PBS and stained with propidium iodide (PI) for 10 min under subdued light. Stained cells were analyzed flow cytometry assay (Becton-Dickinson, NJ, USA), and the results were performed using FCS Express flow cytometry analysis software (ModFit LT 3.1).[28,29]

4.4 Molecular docking study

The crystal structure (PDB: 3GEN) of the kinase domain of BTK bound to a pyrrolopyrimidine-containing compound.[30] The enzyme preparation and the hydrogen atoms adding was performed in the prepared process. The whole BTK enzyme was defined as a receptor and the site sphere was selected on the basis of the binding location of pyrrolopyrimidine inhibitor. By moving the inhibitor and the irrelevant water, molecules **7a**, **7c**, **7l**, **7e**, **7h** and spebrutinib were placed, respectively. The binding interaction energy was calculated to include van der Waals, electrostatic, and torsional energy terms defined in the tripos force field. Ten docking poses were generated and clustered, and compounds with predicted binding affinities better than 7.0 kcal/mol in each of the three docking runs were selected for further analysis and visual inspection. The structure optimization was performed using a genetic algorithm, and only the best-scoring ligand protein complexes were kept for analyses.[31-33] The WWW site also includes many resources for use of AutoDock,

including detailed Tutorials that guide users through basic AutoDock usage, docking with flexible rings, and virtual screening with AutoDock. Tutorials may be found at: <http://autodock.scripps.edu/faqs-help/tutorial>.

Acknowledgments

We are grateful to the National Natural Science Foundation of China (No. 81402788), the project of family noninvasive mechanical ventilation system construction and promotion for AECOPD patients: Health and Family Planning Commission of Liaoning Province (No. 2015B004), the Ph.D. Start-up Fund of Natural Science Foundation of Liaoning Province (No. 20141115), and the Cultivation Project of Youth Techstars, Dalian (2016RQ043) for the financial support of this research.

Reference

- [1] C.M. Lewis, C. Broussard, M.J. Czar, P.L. Schwartzberg, Tec kinases: modulators of lymphocyte signaling and development. *Curr. Opin. Immunol.* 13 (2001) 317–325.
- [2] J.B. Hong, J.P. Davidson, Q. Jin, G.R. Lee, M. Matchett, E. O'Brien, M. Welch, B. Bingenheimer, K. Sarma, Development of a scalable synthesis of a Bruton's tyrosine kinase inhibitor via C–N and C–C bond couplings as an end game Strategy. *Org. Process Res. Dev.* 18 (2014) 228–238.
- [3] X. Zhao, W. Huang, Y. Wang, M. Xin, Q. Jin, J. Cai, F. Tang, Y. Zhao, H. Xiang Discovery of novel Bruton's tyrosine kinase (BTK) inhibitors bearing a pyrrolo [2,3-d] pyrimidine scaffold. *Bioor. Med. Chem.* 23 (2015) 891–901.
- [4] R.C. Rickert, New insights into pre-BCR and BCR signaling with relevance to B cell malignancies. *Nat. Rev. Immunol.* 13 (2013) 578–591.
- [5] R.E. Davis, V.N. Ngo, G. Lenz, P. Tolar, R.M. Young, P.B. Romesser, H. Kohlhammer, L. Lamy, H. Zhao, Y. Yang, W. Xu, A.L. Shaffer, G. Wright, W. Xiao, J. Powell, J.K. Jiang, C.J. Thomas, A. Rosenwald, G. Ott, H.K. Muller-Hermelink, R.D. Gascoyne, J.M. Connors, N.A. Johnson, L.M. Rimsza, E. Campo, E.S. Jaffe, W.H. Wilson, J. Delabie, E.B. Smeland, R.I. Fisher, R.M. Braziel, R.R. Tubbs, J.R. Cook, D.D. Weisenburger, W.C. Chan, S.K. Pierce,

- L.M. Staudt, Chronic active B-cell-receptor signaling in diffuse large B-cell lymphoma. *Nature* 463 (2010) 88–92.
- [6] A. Akinleye, Y. Chen, N. Mukhi, Y. Song, D. Liu, Ibrutinib and novel BTK inhibitors in clinical development. *J. Hematol. Oncol.* 6 (2013) 59–67.
- [7] Z. Pan, H. Scheerens, S.J. Li, B.E. Schultz, P.A. Sprengeler, L.C. Burrill, R.V. Mendonca, M.D. Sweeney, K.C. Scott, P.G. Grothaus, D.A. Jeffery, J.M. Spoerke, L.A. Honigberg, P.R. Young, S.A. Dalrymple, J.T. Palmer, Discovery of selective irreversible inhibitors for Bruton's tyrosine kinase. *ChemMedChem* 2 (2007) 58–61.
- [8] L.A. Honigberg, A.M. Smith, M. Sirisawad, E. Verner, D. Loury, B. Chang, S. Li, Z. Pan, D.H. Thamm, R.A. Miller, J.J. Buggy, The Bruton tyrosine kinase inhibitor PCI-32765 blocks B-cell activation and is efficacious in models of autoimmune disease and B-cell malignancy. *Proc. Natl. Acad. Sci. USA.* 107 (2010) 13075–13080.
- [9] M. F. de Rooij, A. Kuil, C. R. Geest, E. Eldering, B. Y. Chang, J. J. Buggy, S. T. Pals, M. Spaargaren, The clinically active BTK inhibitor PCI-32765 targets B-cell receptor- and chemokine-controlled adhesion and migration in chronic lymphocytic leukemia. *Blood* 119 (2012) 2590–2594.
- [10] J.C. Byrd, B. Harrington, S. O'Brien, J.A. Jones, A. Schuh, S. Devereux, J. Chaves, W.G. Wierda, F.T. Awan, J.R. Brown, P. Hillmen, D.M. Stephens, P. Ghia, J.C. Barrientos, J.M. Pagel, J. Woyach, D. Johnson, J. Huang, X. Wang, A. Kaptein, B.J. Lannutti, T. Covey, M. Fardis, J. McGreivy, A. Hamdy, W. Rothbaum, R. Izumi, T.G. Diacovo, A.J. Johnson, R.R. Furman, Acalabrutinib (ACP-196) in relapsed chronic lymphocytic leukemia. *N. Engl. J. Med.* 374 (2016) 323–332.
- [11] B.K. Harrington, H.L. Gardner, R. Izumi, A. Hamdy, W. Rothbaum, K.R. Coombes, T. Covey, A. Kaptein, M. Gulrajani, B. Van Lith, C. Krejsa, C.C. Coss, D.S. Russell, X. Zhang, B.K. Urie, C.A. London, J.C. Byrd, A. J. Johnson, W.C. Kisseberth. Preclinical Evaluation of the novel BTK inhibitor

- Acalabrutinib in canine models of B-Cell non-Hodgkin lymphoma. *PLoS One* 11 (2016) e0159607.
- [12] J. Wu, M. Zhang, D. Liu, Acalabrutinib (ACP-196): a selective second-generation BTK inhibitor. *J. Hematol. Oncol.* 9 (2016) 1–4.
- [13] H.S. Walter, S.A. Rule, M.J. Dyer, L. Karlin, C. Jones, B. Cazin, P. Quittet, N. Shah, C.V. Hutchinson, H. Honda, K. Duffy, J. Birkett, V. Jamieson, N. Courtenay-Luck, T. Yoshizawa, J. Sharpe, T. Ohno, S. Abe, A. Nishimura, G. Cartron, F. Morschhauser, C. Feqan, G. Salles, A phase 1 clinical trial of the selective BTK inhibitor ONO/GS-4059 in relapsed and refractory mature B-cell malignancies. *Blood* 127 (2016) 411–419.
- [14] R. Jones, M.J. Axelrod, D. Tumas, C. Queva, J.D. Paolo, Combination effects of B cell receptor pathway inhibitors (Entospletinib, ONO/GS-4059, and Idelalisib) and a BCL-2 inhibitor in primary CLL cells. *Blood* 126 (2016) 1749.
- [15] E. Evans, S. Ponader, R. Karp, R. Tester, M. Sheets, S. Aslanian, T. St. Martin, M. Nacht, Z. Zhu, P. Chaturvedi, S. Witowski, H. Lounsbury, K. Stiede, J. Burger, R. Petter, J. Singh, W. F. Westlin, Covalent inhibition of Btk with clinical development compound AVL-292 disrupts signaling that maintains the microenvironment necessary for chronic lymphocytic leukemia growth *Clin. Lymphoma Myeloma Leuk.* 11 (2011) S173–S174.
- [16] J.K. Park, J.Y. Byun, J.A. Park, Y.Y. Kim, Y.J. Lee, J.I. Oh, S.Y. Jang, Y.H. Kim, Y.W. Song, J. Son, K.H. Suh, Y.M. Lee, E.B. Lee, HM71224, a novel Bruton's tyrosine kinase inhibitor, suppresses B cell and monocyte activation and ameliorates arthritis in a mouse model: a potential drug for rheumatoid arthritis *Arthritis. Res. Ther.* 18 (2016) 91–99.
- [17] X. Li, Y. Zuo, G. Tang, Y. Wang, Y. Zhou, X. Wang, T. Guo, M. Xia, N. Ding, Z. Pan, Discovery of a series of 2,5-diaminopyrimidine covalent irreversible inhibitors of Bruton's tyrosine kinase with in vivo antitumor activity. *J. Med. Chem.* 57 (2014) 5112–5128.
- [18] H. Wu, W. Wang, F. Liu, E.L. Weisberg, B. Tian, Y. Chen, B. Li, A. Wang, B. Wang, Z. Zhao, D.W. McMillin, C. Hu, H. Li, J. Wang, Y. Liang, S.J. Buhrlage, J. Liang, J. Liu, G. Yang, J.R. Brown, S.P. Treon, C.S. Mitsiades, J.D. Griffin, Q.

- Liu, N.S. Gray, Discovery of a potent, covalent BTK inhibitor for B-cell lymphoma. *ACS Chem. Biol.* 9 (2014) 1086–1091.
- [19] L. Santos-Garcia, L.C. Assisa, D.R. Silva, T.C. Ramalho, E.F. da Cunha, QSAR analysis of nicotinamidic compounds and design of potential Bruton's tyrosine kinase (Btk) inhibitors. *J. Biomol. Struct. Dyn.* 34 (2016) 1421–1440.
- [20] A. Xu, Y. Zhang, T. Ran, H. Liu, S. Lu, J. Xu, X. Xiong, Y. Jiang, T. Lu, Y. Chen, Quantitative structure-activity relationship study on BTK inhibitors by modified multivariate adaptive regression spline and CoMSIA methods. *SAR. QSAR Environ. Res.* 26 (2015) 279–300.
- [21] W. Zhou, D. Ercan, L. Chen, C.H. Yun, D. Li, M. Capelletti, A.B. Cortot, L. Chirieac, R.E. Jacob, R. Padera, J.R. Engen, K.K. Wong, M.J. Eck, N.S. Gray, P.A. Jänne, Novel mutant-selective EGFR kinase inhibitors against EGFR T790M. *Nature* 462 (2009) 1070–1074.
- [22] C. Han, Z. Huang, C. Zheng, L. Wan, L. Zhang, S. Peng, K. Ding, H. Ji, J. Tian, Y. Zhang, Novel hybrids of (phenylsulfonyl)furoxan and anilinopyrimidine as potent and selective epidermal growth factor receptor inhibitors for intervention of non-small-cell lung cancer. *J. Med. Chem.* 56 (2013) 4738–4748.
- [23] G.F. Manbeck, A.J. Lipman, R.A. Stockland, A.L. Freidl, A.F. Hasler, J.J. Stone, I.A. Guzei, Organosoluble copper clusters as precatalysts for carbon-heteroelement bond-forming reactions: Microwave and conventional heating. *J. Org. Chem.* 70 (2005) 244–250.
- [24] Y. Tong, T.D. Penning, A.S. Florjancic, J. Miyashiro, K.W. Woods, Preparation of substituted fused tricycles as inhibitors of kinases for treating cancer, *Patent*, WO2012161812A1. 2012.
- [25] J.V. Cizdziel, C. Tolbert, G. Brown, Direct analysis of environmental and biological samples for total mercury with comparison of sequential atomic absorption and fluorescence measurements from a single combustion event. *Spectrochim. Acta Part B At. Spectros.* 65 (2010) 176–180.
- [26] R. Somberg, B. Pferdehirt, A.K. Kupcho, Kinase-Glo luminescent kinase assay: detect virtually any kinase. *Cell Notes.* 5 (2003) 5–8.
- [27] H. Zegzouti, M. Zdanovskaia, K. Hsiao, S.A. Goueli, ADP-Glo: A Bioluminescent and homogeneous ADP monitoring assay for kinases. *Assay*

- Drug Dev. Technol.* 7 (2009) 560–572.
- [28] K.C. Kawabata, S. Ehata, A. Komuro, K. Takeuchi, K. Miyazono, TGF-beta-induced apoptosis of B-cell lymphoma Ramos cells through; reduction of MS4A1/CD20. *Oncogene* 32 (2013) 2096–2106.
- [29] Y. Azuma, M. Sakanashi, K. Matsumoto, The effect of alpha 2,6-linked sialic acid on anti-IgM antibody-induced apoptosis in Ramos cells. *Glycoconj. J.* 18 (2001) 419–424.
- [30] D.J. Marcotte, Y.T. Liu, R.M. Arduini, C.A. Hession, K. Miatkowski, C.P. Wildes, P.F. Cullen, V. Hong, B.T. Hopkins, E. Mertsching, T.J. Jenkins, M.J. Romanowski, D.P. Baker, L.F. Silvan, Structures of human Bruton's tyrosine kinase in active and inactive conformations suggest a mechanism of activation for TEC family kinases. *Protein Sci.* 19 (2010) 429–439.
- [31] S.A. Wildman, X. Zheng, D. Sept, J.T. Auletta, T. L. Rosenberry, G. R. Marshall, Drug-like leads for steric discrimination between substrate and inhibitors of human acetyl cholinesterase. *Chem. Biol. Drug Des.* 78 (2011) 495–504.
- [32] G.M. Morris; R. Huey, W. Lindstrom, M.F. Sanner, R.K. Belew, D.S. Goodsell, A.J. Olson, AutoDock4 and AutoDockTools4: Automated docking with selective receptor flexibility. *J. Comput. Chem.* 30 (2009) 2785–2791.
- [33] D.S. Goodsell, G. M. Morris, A.J. Olson, Automated docking of flexible ligands: applications of autodock. *J. Mol. Recognit.* 9 (1996) 1–5.

Fig. 1.

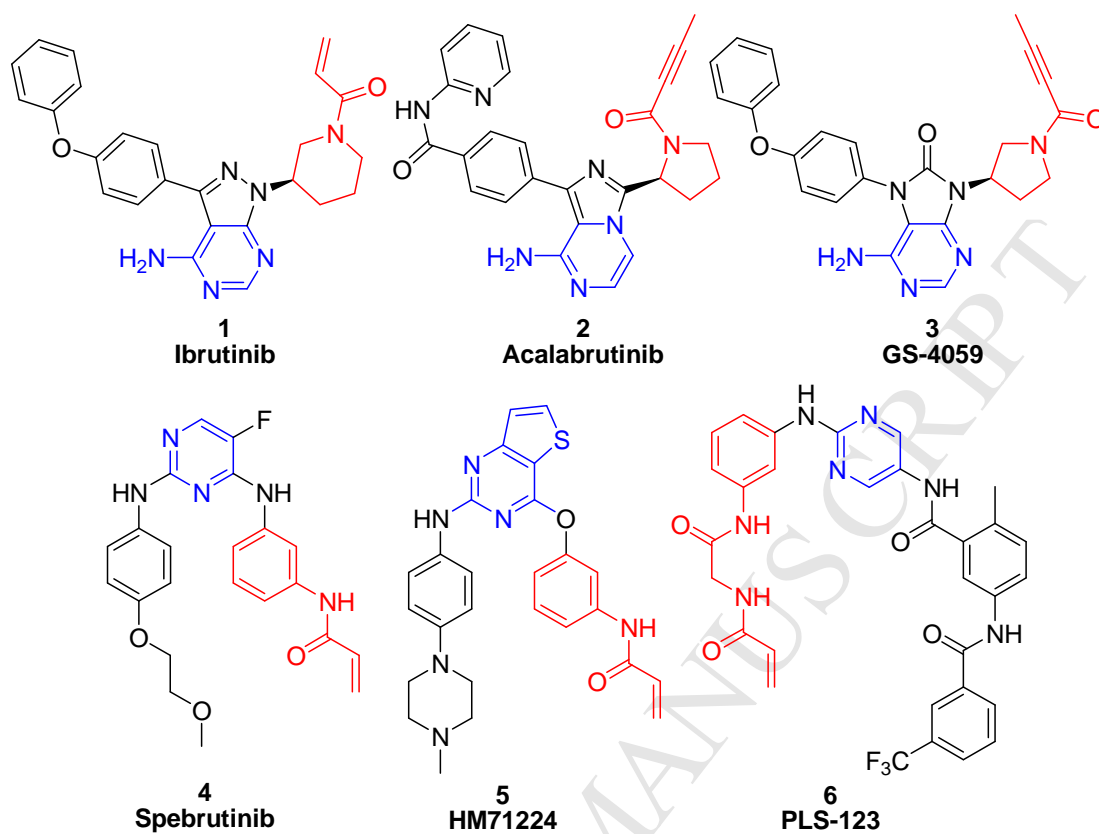


Fig. 2.

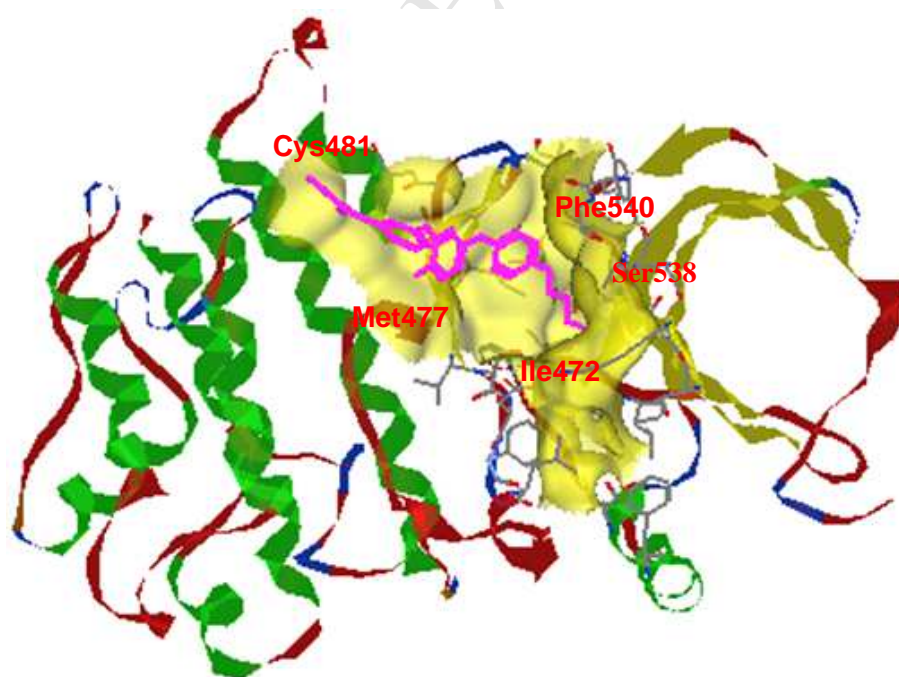


Fig. 3.

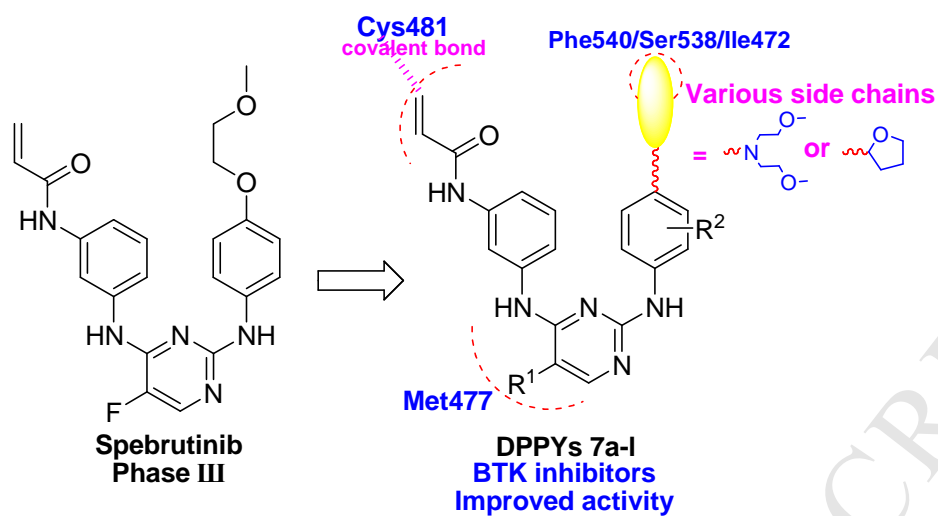


Fig. 4.

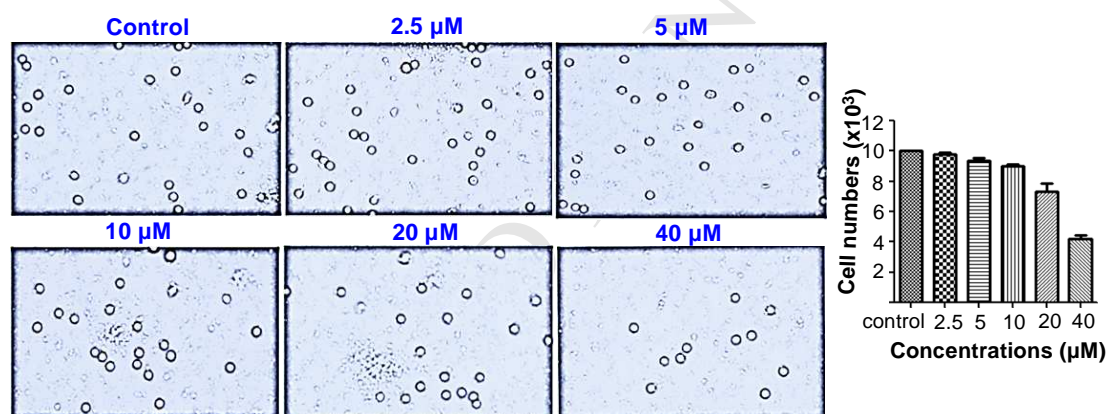


Fig. 5.

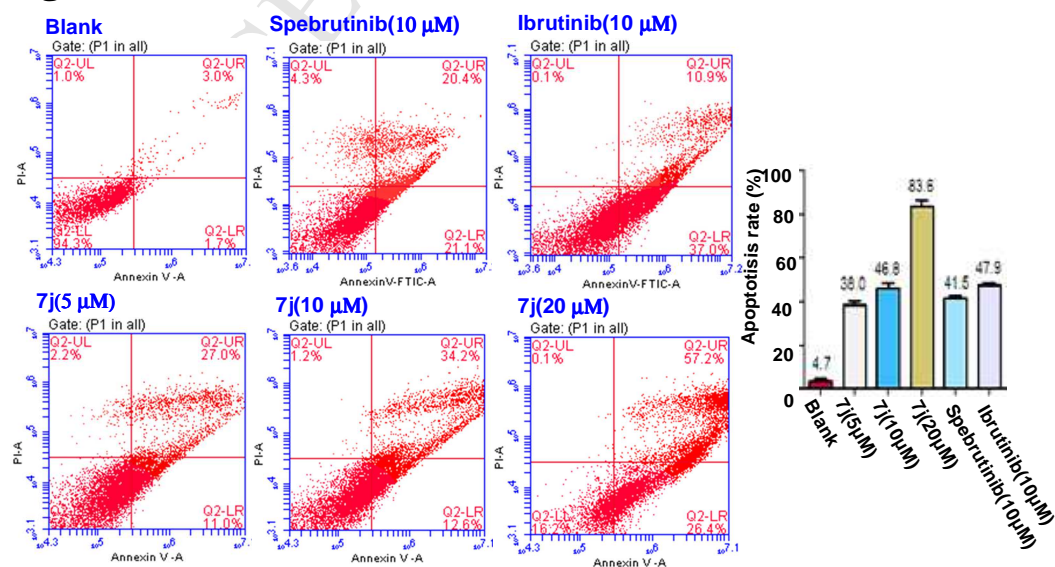


Fig. 6.

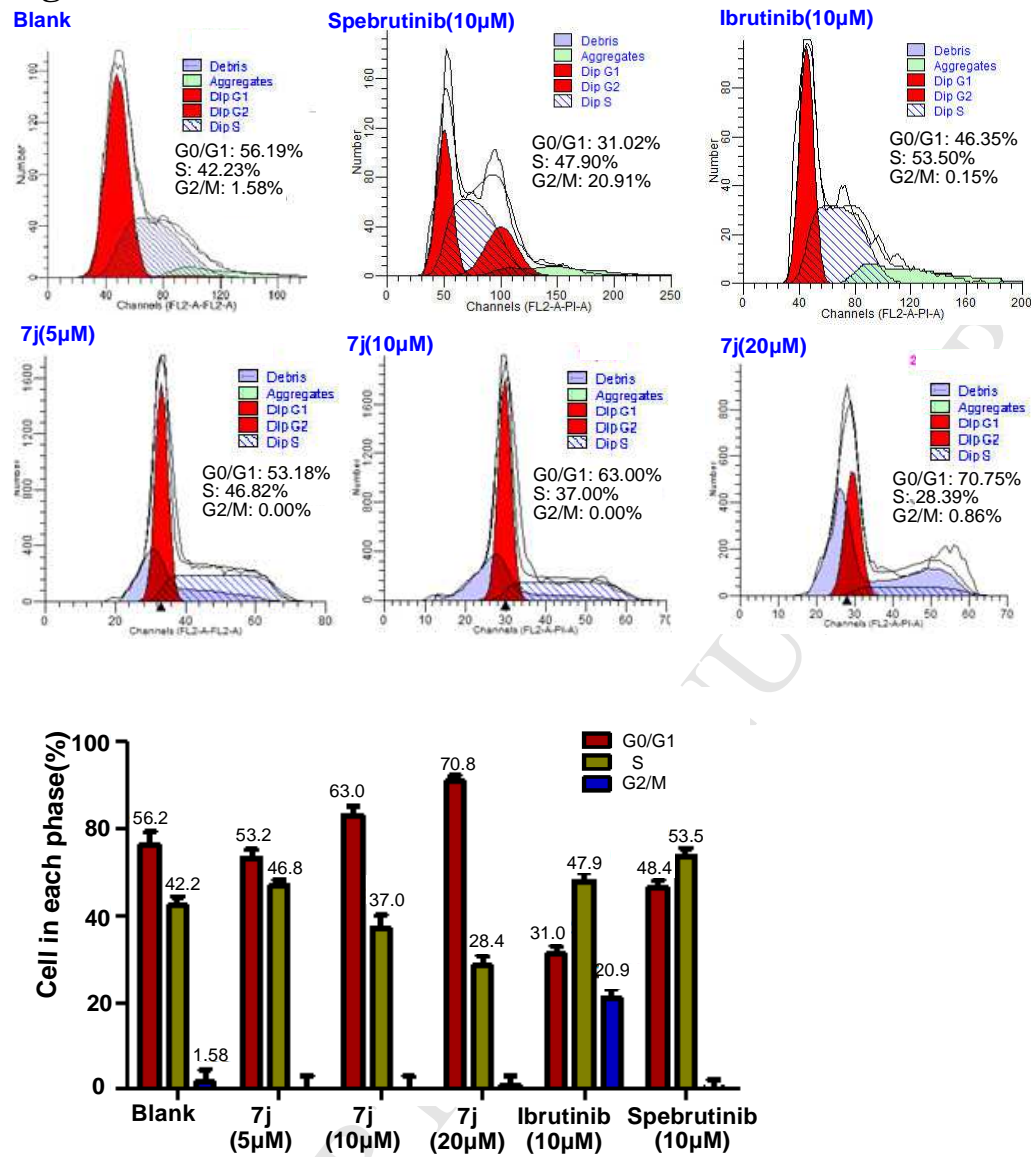
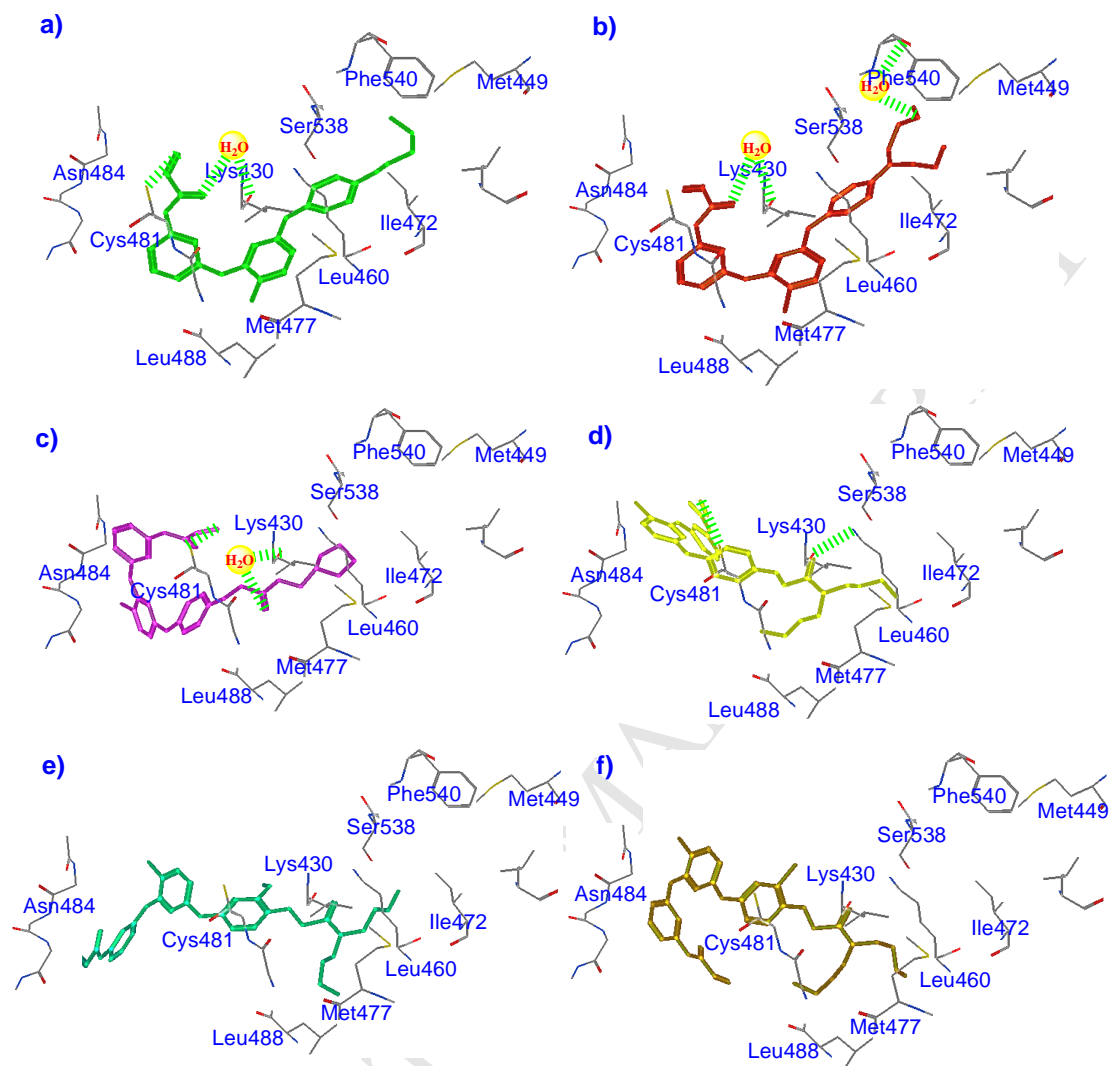
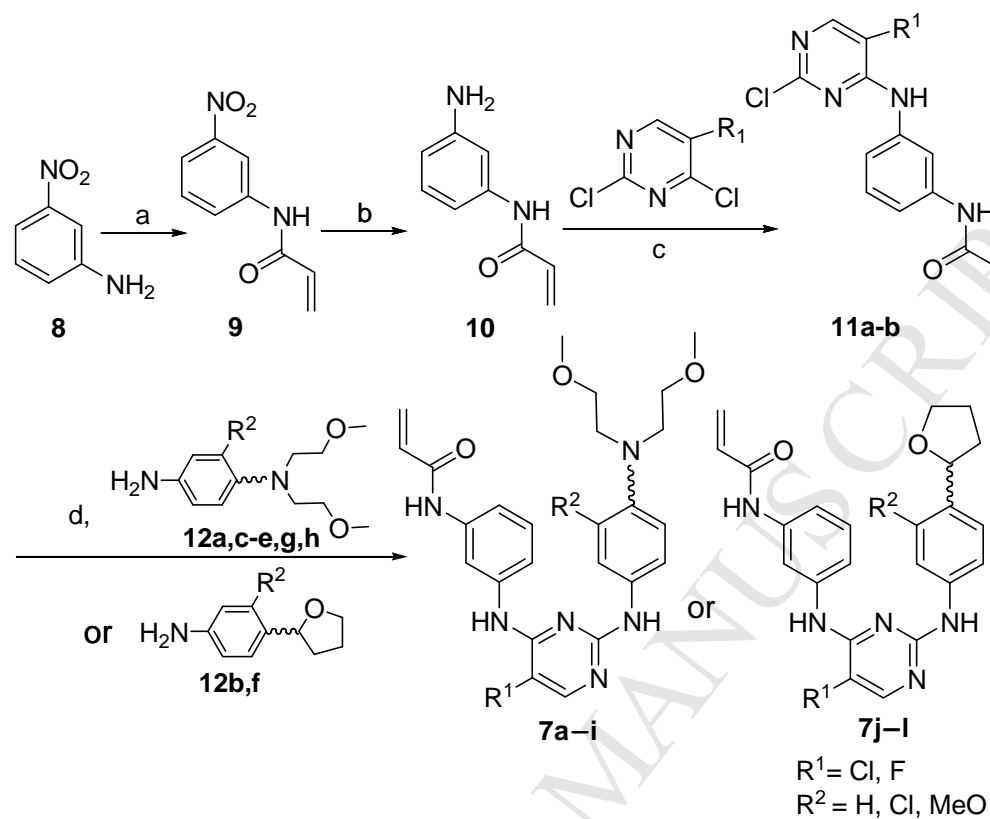


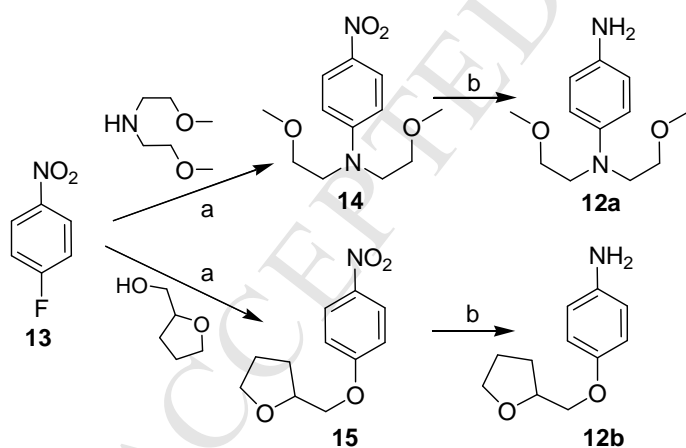
Fig. 7.



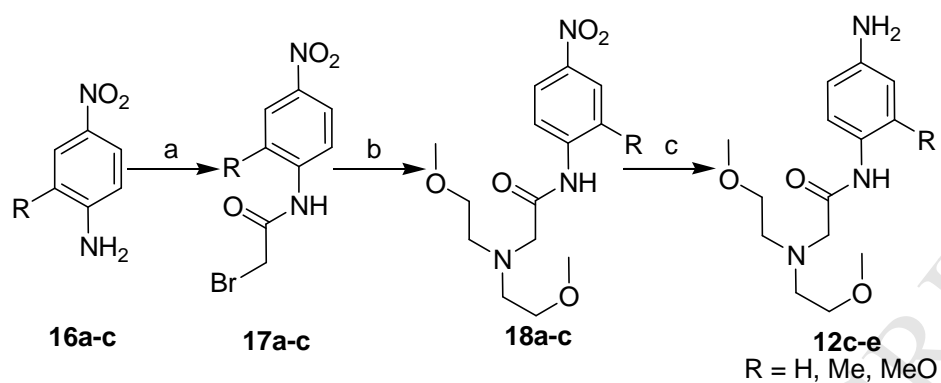
Scheme 1.



Scheme 2.



Scheme 3.



Scheme 4.

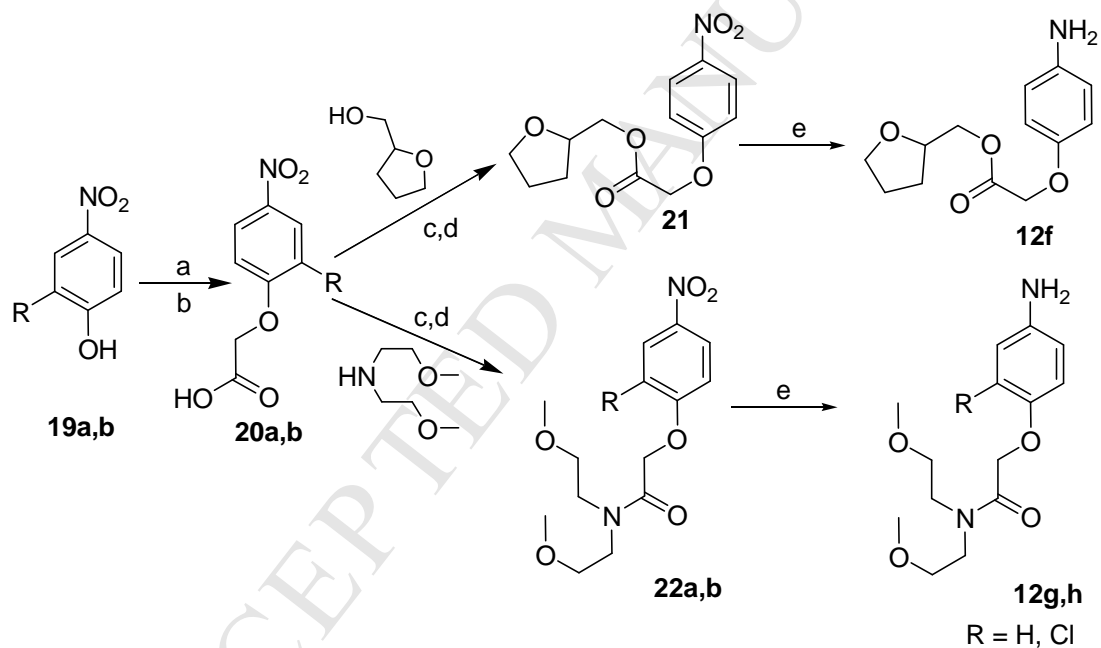
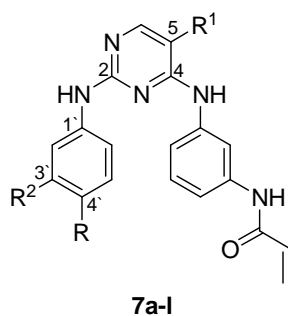


Table 1



Compound	5-R ¹	3'-R ²	4'-R	Enzymatic activity (IC ₅₀ , nM)	Antiproliferative activity (IC ₅₀ , μM) ^b	
				BTK	Ramos	Raji
7a	Cl	H		4.94	13.0	30.5
7b	F	H		7.12	18.1	23.8
7c	Cl	H		2.83	18.1	20.1
7d	F	H		27.2	>40.0	36.0
7e	Cl	Cl		>100	16.9	19.3
7f	Cl	H		22.6	14.8	19.9
7g	F	H		91.3	35.6	36.9
7h	Cl	OMe		>100	11.0	20.9
7i	Cl	Me		20.0	19.6	35.6
7j	Cl	H		12.1	10.5	19.1
7k	F	H		22.4	22.3	38.6
7l	Cl	H		0.23	>40	9.4
Spebrutinib				0.72	20.9	29.4
Ibrutinib				0.34	12.6	19.3

Table 2

	Times	Control ^a	Normal BTK ^b	Inhibitor-linked BTK ^c
Luminescence values	1	166	9702	430
	2	180	10652	412
	3	208	9574	308
	Ave.	185	9976	383

Fig. 1. Structures of the novel BTK inhibitors.

Fig. 2. Binding mode of spebrutinib with BTK enzyme (PDB: 3GEN).

Fig. 3. Designed strategy of new DPPYs as potent BTK inhibitors.

Fig. 4. Morphological changes of the PBMC cells treated by molecule **7j** (100 ×, final magnification) at concentration of 2.5, 5, 10, 20, 40 μM for 24 h. Cell numbers were calculated by traditional manual method with an ordinary cell counting chamber. One representative experiment is shown.

Fig. 5. Compound **7j** induced Ramos cell apoptosis *in vitro*. The cells were incubated with the indicated concentrations of **7j** for 48 h, and the cells were stained with annexin V/FTIC, followed by flow cytometry analysis. One representative experiment is shown. $p < 0.05$.

Fig. 6. Effects of spebrutinib, ibrutinib and **7j** on Ramos cell cycle arrest detected by flow cytometry assay. Results are representative of three separate experiments, dates are expressed as the mean±standard deviation, $p < 0.05$.

Fig. 7. a) Putative binding mode of spebrutinib within BTK (PDB code: 3GEN); b) Putative binding mode of inhibitor **7a** within BTK (PDB code: 3GEN); c) Putative binding mode of inhibitor **7l** within BTK (PDB code: 3GEN); d) Putative binding mode of inhibitor **7c** within BTK (PDB code: 3GEN); e) Putative binding mode of inhibitor **7e** within BTK (PDB code: 3GEN); f) Putative binding mode of inhibitor **7h** within BTK (PDB code: 3GEN).

Scheme 1. Synthetic route of title compounds **7a-l**. Reagents and conditions: (a) acryloyl chloride, NaHCO₃, CH₃CN, rt, 0.5 h, 95%; (b) Fe-NH₄Cl, MeOH-H₂O, 2 h, 70 °C, 72%; (c) ArNH₂, DIPEA, 1,4-dioxane, 60 °C, 2 h, 91%; (d) trifluoroacetic acid, intermediates **12a-h**, 2-BuOH, 100 °C, 12 h, 31% to 45%.

Scheme 2. Synthetic route of intermediates **12a,b**. Reagents and conditions: (a) K₂CO₃, CH₃CN, 80 °C, 12 h, 63-85%; (b) Fe-NH₄Cl, MeOH-H₂O, 2 h, 70 °C, 60-87%.

Scheme 3. Synthetic route of intermediates **12c-e**. Reagents and conditions: (a) bromoacetyl bromide, NaHCO₃, CH₃CN, rt, 0.5 h, 93%; (b) bis(2-methoxyethyl)amine, K₂CO₃, CH₃CN, 80 °C, 12 h, 71-88%; (c) Fe-NH₄Cl, MeOH-H₂O, 2 h, 70 °C, 63-82%.

Scheme 4. Synthetic route of intermediates **12f-h**. Reagents and conditions: (a) ethyl bromoacetate, K₂CO₃, CH₃CN, rt, 5 h, 91%; (b) KOH, MeOH-H₂O, 50 °C, 1 h, 62-78%; (c) (COCl)₂, 50 °C, 1 h; (d) K₂CO₃, CH₃CN, 80 °C, 12 h, 55-78%; (e) Fe-NH₄Cl, MeOH-H₂O, 2 h, 70 °C, 61-72%.

Table 1 Biological activity of the newly synthesized DPPYs.^a

^aData represent the mean of at least three separate experiments. ^bDose-response curves were determined at five concentrations. The IC₅₀ values are the concentrations in micromolar needed to inhibit cell growth by 50% as calculated using GraphPad Prism version 5.0.

Table 2 The luminescence values produced by treating BTK, and inhibitor-linked BTK with ADP-Glo™ Kinase Assay system.

^a3 μL 1 \times buffer, 2 μL (0.5 $\mu\text{g}/\mu\text{L}$ substrate, 125 μM ATP); ^b1 μL 1 \times buffer, 2 μL (0.5 $\mu\text{g}/\mu\text{L}$ substrate, 125 μM ATP), 2 μL 2.5 ng/ μL enzyme; ^c1 μL 500 nmol/L drug, 2 μL (0.5 $\mu\text{g}/\mu\text{L}$ substrate, 125 μM ATP), 2 μL 2.5 ng/ μL enzyme.

- A new series of DPPYs were synthesized and biologically evaluated as potent BTK inhibitors.
- DPPYs could inhibit BTK activity at nanomolar concentrations.
- Inhibitor **7j** displayed higher inhibitory capacity to interfere with B leukemia cell lines than ibrutinib.
- Inhibitor **7j** has low cell cytotoxicity against normal PBMC cells.